MEMORANDUM
RM-5685-PR
JUNE 1968

MORE NUCLEAR EXPLOSIONS IN CAVITIES

H. L. Brode

PREPARED FOR:
UNITED STATES AIR FORCE PROJECT RAND

The RAND Corporation
SANTA MONICA • CALIFORNIA

MEMORANDUM
RM-5685-PR
JUNE 1968

MORE NUCLEAR EXPLOSIONS IN CAVITIES

H. L. Brode

This research is supported by the United States Air Force under Project RAND — Contract No. F11620-67-C-0015 — monitored by the Directorate of Operational Requirements and Development Plans, Deputy Chief of Staff, Research and Development, Hq USAF. RAND Memoranda are subject to critical review procedures at the research department and corporate levels. Views and conclusions expressed herein are nevertheless the primary responsibility of the author, and should not be interpreted as representing the official opinion or policy of the United States Air Force or of The RAND Corporation.

The RAND Corporation
1700 MAIN ST • SANTA MONICA • CALIFORNIA • 90406

PREFACE

The use of underground cavities to muffle or seismically decouple nuclear explosions could drastically complicate the problems of detecting seismic signals from such bursts. Much of the early theoretical effort on decoupling, done here at RAND, has proven useful and valid. Recent interest has centered on more sophisticated muffling techniques, using special materials in the underground cavities to reduce the late-time pressures. The set of calculations reported on in this memorandum extends an earlier set to larger cavities and to cavities containing low density water vapor.

SUMMARY

Low yield nuclear explosions in partially evacuated underground cavities cause complex loads on the rock walls (but in general lead to much reduced distant seismic signals). An earlier set of calculations describe cavity gas dynamics and wall pressures and temperatures for 1.7 KT in 20 and 40 meter radius cavities with normal density air, and with one-tenth and one-hundredth of normal density air inside. The present memorandum extends these to cavities of 40, 60 and 80 meters radius, and to a contained atmosphere of water vapor at around 11 torr.

CONTENTS

I. INTRODUCTION

Renewed interest in nuclear explosions in underground cavities for the purpose of minimizing the seismic signal from such tests has prompted a few further calculations similar to earlier reported ones.[1] Since the earlier calculations were undertaken (1958), supporting the original theoretical development of the notion of seismic decoupling,[2-5] relatively little further sophistication has been incorporated in the theory. This may be attributable to the fact that little doubt remains as to the feasibility of decoupling by means of large underground cavities, and that the attenuated signals would complicate the inspection and policing of any treaty banning underground nuclear tests. However, some question remains about the practicality of decoupling by means of large excavated cavities and that question has prompted some further look at ways of reducing the required cavity size and depth. The most promising of these attempt to reduce the average cavity pressure with energy absorbers in the cavity.[6]

The additional calculations reported here do not include the effects of absorbers, but rather extend the previous results to larger cavity sizes, to lower ambient (pre-shot) cavity pressures, and to higher yields. A major difference is that the cavity gas is considered to be water vapor, since in a practical, unlined cavity pumping out the air is likely to be limited to the vapor pressure of water at the ambient temperature of the cavity rock.

II. THE PHYSICAL MODEL

As discussed in earlier reports,[1,7] the assumptions of spherical symmetry, thermodynamic equilibrium, radiation diffusion, and hydrodynamics are quite appropriate to the early phases of nuclear explosions in gaseous atmospheres.

The previous model assumed that wall response was negligible and could reasonably be taken as rigid and non-absorbing as far as the description of the cavity gas dynamics was concerned. Since for the low yields of these examples (1.7 and 10 KT) radiative wall losses are not likely to be a dominant feature, little effort was made to account for such losses in detail. Instead, the first few hundred calories per square centimeter were allowed to leak out of the growing fireballs (representing heat to the wall surfaces), but such loss was later cut off on the presumption that the wall surfaces could by then have reached equilibrium with the cavity gas temperature, and that further loss would rely on thermal diffusion within the rock walls themselves. Thermal conductivity in nearly all rock is too slow to be a factor in cavity dynamics over the times of interest here (fractions of a second).

The explosive source was taken as a sphere of aluminum. (One case was done with half the initial mass.) An energy of 7.1×10^{19} ergs (1.7 KT) was dumped into the aluminum in a fraction of a microsecond. Although such a source does not represent the right materials, and may be too low a yield to be of greatest interest, it does provide direct comparison with the previous calculations.[1]

The equation of state and opacity used for the aluminum was as follows.

EQUATION OF STATE FOR ALUMINUM

$\eta = v_o/v$, $s = .0299979$, $v_o = .36900369$

v = specific volume (cm^3/gm), T = temperature (10^4 ^oK).

Pressure:

for

$$\eta < 1; \quad P = \frac{48T\eta^{.907}\,(1 + .004T)(T-S)}{\left(T + \frac{10(1-\eta)}{1+50\,\eta^2}\right)\left(\frac{2000(1-\eta)^3\eta}{1+T^2}+1\right)}, \quad (\text{jerks/m}^3) \qquad (1)$$

for

$$\eta \geq 1; \quad P = 48(T-S)(1 + .004T)\eta^{.8} + 278\eta(\eta^{1/3}-1)\eta^{1/3}.$$

Internal Energy:

for

$$\eta < 1; \quad E = \frac{11T^{1.16}\left(1 + \frac{.055T}{\eta^{.5}}\right)}{1 + .01T\left(1 + \frac{1}{\eta^{.5}}\right)}, \quad (\text{jerks/Mg}) \qquad (2)$$

for

$$\eta \geq 1; \quad E = 307.749\left[(.5\eta^{1/3}-1)\eta^{1/3}+.5\right] + \left(\frac{2.656641 + .3542434T^2}{\eta^{.2}}\right) - 2.656641 + 11T^{1.16}.$$

The Rosseland mean opacity:

$$k = 2.25\text{x}10^4 + \frac{2\text{x}10^6(1+2.37\text{x}10^{-17}T^5)}{V(1+.817\text{x}10^{-17}T^6)} + \frac{4.23\text{x}10^9T^2}{V^{.5}(1+.02T^3+1.76\text{x}10^{-7}T^6)}$$

$$\left(\frac{\text{m}^4(10^4\ ^{\circ}\text{K})^4\text{msec}}{\text{Mg.jerk}}\right) \qquad (3)$$

$k = \frac{3}{ac} K_R$, K_R Rosseland mfp (cm^2/g), $a = 7.62^{-15}$ erg/cm^3/deg^4,

c = velocity of light.

The cavities were assumed to contain only water vapor at an initial temperature of 286.5 ^{o}K, and at the low density of 1.18 x 10^{-5} gm/cm^3. Since no simple analytic fit for the equation of state of water was available to us, it was necessary to invent one. The following formulae for pressure and energy are based on the equation of state work of Gilmore,[8] Papetti and Fujisaki,[9] and Krieger[10] at RAND. Credit for the derivation of the fit must go largely to Anne Stevenson and Wakichi Asano. Although the pressure and internal energy fits are based on the thermodynamic quantities for water, the Rosseland mean opacity is the same as that for air. With Gilmore's concurrence, this approximation was justified on the basis that radiation plays only a secondary role in the cavity dynamics for the yields and cavity sizes chosen, and the air and water opacities should be quite similar in the temperature and density region of interest. If it should later be determined that radiation diffusion is of more importance, then further attention should be given to deriving adequate opacities for water.

EQUATION OF STATE FOR WATER

$$\tau = TV^{.095}, \quad \alpha = TV^{.0602}, \quad \eta = v_o/v, \quad v_o = 773.395$$

Pressure:

$$P = \frac{4.6165T}{v}\left[\left(1 + \frac{2\tau^7}{.058V^{.285} + \tau^7} + \frac{3\tau^5}{1500V^{.095} + \tau^5}\right) + \left(\frac{5\tau^3}{17500T + \tau^3} + \frac{2\tau^5}{5 \times 10^6 + \tau^5}\right)\right] \quad (\text{jerks/m}^3). \qquad (4)$$

Internal Energy:

$$E = 4.6165T\left[\frac{2.9+2T}{1+.1T} + \frac{314.456\alpha^6}{1+12.55\alpha^7}\,\frac{.17364\alpha^4}{1+3.1652\times10^{-4}\alpha^6} + \frac{.0038141\alpha^4}{1+4.9456\times10^{-6}\alpha^6}\right.$$

$$\left. + \frac{.0576349\alpha^2}{1+9.539\times10^{-7}\alpha^4} + \frac{7.533\times10^{-12}\alpha^6}{1+1.589\times10^{-15}\alpha^7}\right] \quad \text{(jerks/Mg)}. \qquad (5)$$

Rosseland (diffusion) Mean Opacity:

$$k = 1321.2V/(E+F+G+H) \qquad \left(\frac{\text{in}^4(10^4\ {}^{o}\text{K})^4\text{msec}}{\text{Mg.jerk}}\right) \qquad (6)$$

$$A = \frac{0.912}{2.5\eta+.51\eta^2} + \frac{5.3\times10^{-5}}{\eta^3}, \qquad B = \frac{.01075}{\eta(1+.025\eta)} + 1.995\times10^{-6}\eta^3,$$

$$C = 10^{-6}\left[\frac{.7767}{\eta} + \frac{3.933}{\eta^2} + \frac{1.3}{\eta^3}\right], \qquad D = \frac{C}{T^8}, \qquad E = \frac{A}{B+D+T^8},$$

$$F = \frac{.01\eta^{-1.5}T^6}{1+T^8}, \qquad G = \frac{.0003\eta^{-1.82}T^6}{2+T^6},$$

$$H = \left(\frac{1+1.16\times10^{-9}\eta\beta T^4}{1+1.65\times10^{-8}\eta\beta T^4}\right)\cdot\left(\frac{2.28\times10^{-8}\eta^{-1.72}T^4}{1+3.82\times10^{-11}\eta^{-.72}T^4}\right),$$

and

$\beta = -.3$ if $\eta \leq 1$, $\beta = +.3$ if $\eta > 1$.

Planck (emission) Mean Free Path:

$$\lambda_E = \frac{0.24\times10^{-3}}{\eta}\left[\frac{1+\frac{1}{100\eta}}{T^{12}} + \frac{10^3}{\eta^{1/3}T^4}\right]$$

for $10^{-4} < \eta < 10$ and $0.2 \leq T \leq 1$ (m)

III. THE MATHEMATICAL MODEL

Extensive descriptions of the numerical methods and the mathematical model for such radiation diffusion and hydrodynamic problems are available elsewhere.[7] The program used here, like that used for earlier calculations, treats hydrodynamics and radiation diffusion in spherical symmetry. An all-FORTRAN version is being used at several laboratories. The present set of calculations was accomplished on the RAND IBM 7044 in about thirty hours. (According to sample test runs, on a Control Data 6400 or 6600 machine that would amount to little more than an hour of machine time.)

The code uses an artificial viscosity to smear shock fronts over a few zones -- thus avoiding discontinuities which would require special handling in a finite difference method such as this. It otherwise integrates the differential equations of motion and transport (in the diffusion and grey-body limits) by successive time increments in the corresponding system of difference equations. All the features used in these calculations are described in detail in Ref. 7 where test problems and a code listing are given.

IV. RESULTS

THE SIXTY METER CAVITY

The pressure on the wall of the 60 m radius cavity is shown as a function of time in Fig. 1. The first step in the initial rise of pressure (at about 35 kb) corresponds to the arrival of the radiation-driven front in the water vapor, while the spike that follows (rising to 157 bars) results from the case shock. The wall pressure drops as the reflected shock implodes on the cavity center again and comes back out. The minimum is around ten kilobars and the second shock on the wall rises only to 32.7 kb. The time between shocks is 4.6 msec.

Densities at the wall are shown in Fig. 2 as a function of time. The mild reflection of the radiation front suggests that it is partially shocked up. As evidence that motion is occurring, note that the density rises from an ambient value of 11.79 gm/m^3 to 33.41 gm/m^3 as the radiation front reflects. The peak compression due to the case shock reflection runs to nearly ten times the pre-shot ambient. During the implosion phase (when the reflected shock is returning toward the center), the gas density at the wall drops to nearly half of the pre-shot ambient.

Temperatures near the wall (Fig. 3) show a rise to more than 37,000 ^{o}K in the arrival of the radiation front, and a peak of nearly 55,000 ^{o}K when the case shock reaches the wall. Although the temperature drops as the reflected shock moves in on the origin, it begins to rise again before the shock returns because of the continued radiation diffusion.

Pressure profiles at times before first reflection and until after the second wall reflection are shown in Fig. 4. It is clear that the pressure is quickly equalizing throughout the cavity. The temperature profiles in Fig. 5 at the same times show a corresponding trend toward a uniform temperature. Figure 6 gives corresponding density profiles.

At about .75 msec, the wall loss was turned off. Until that time, the grey-body loss mechanism using the Planck mean free path

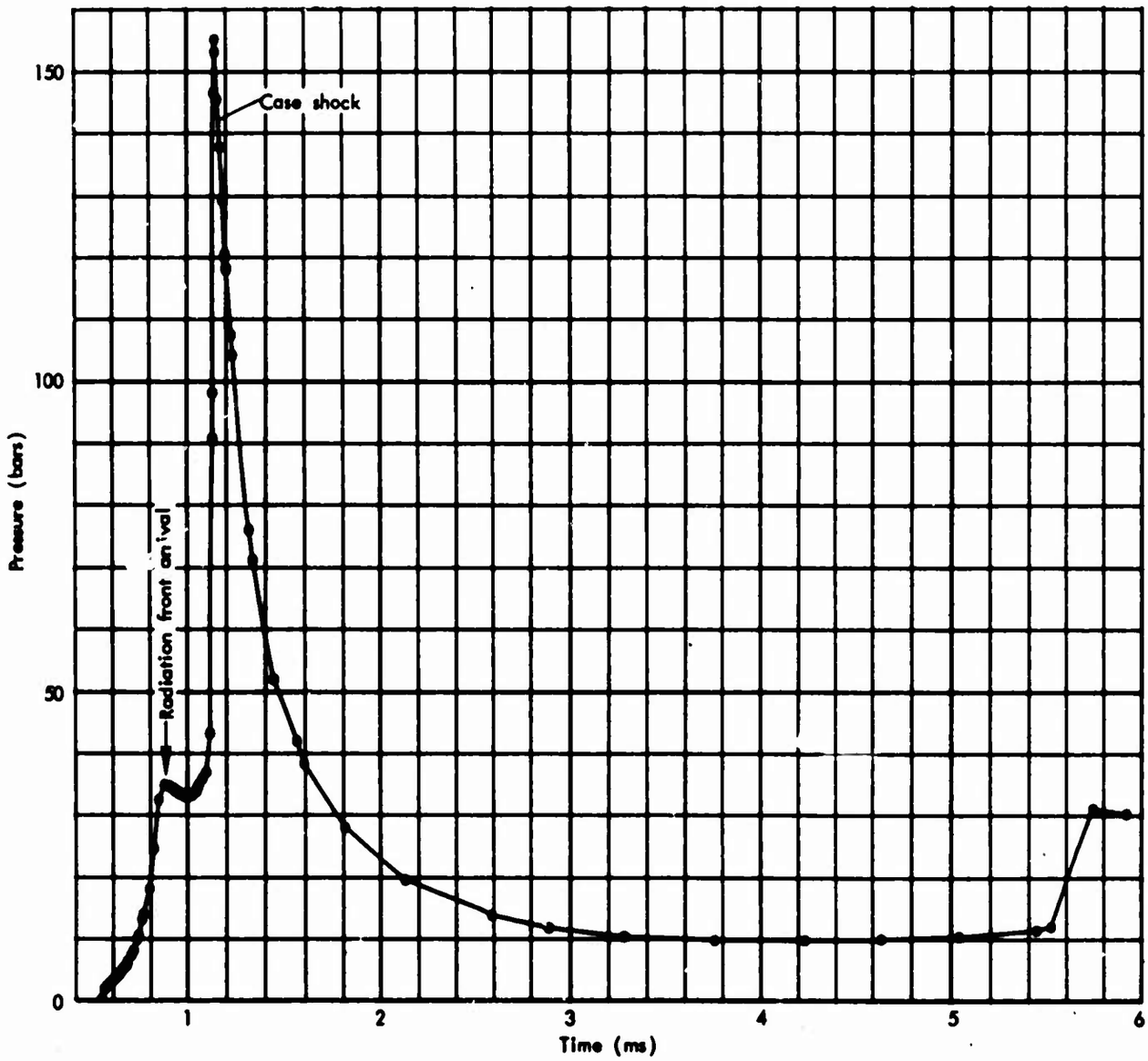

Fig. 1—Wall pressure versus time, 60 m radius, 1.7 KT

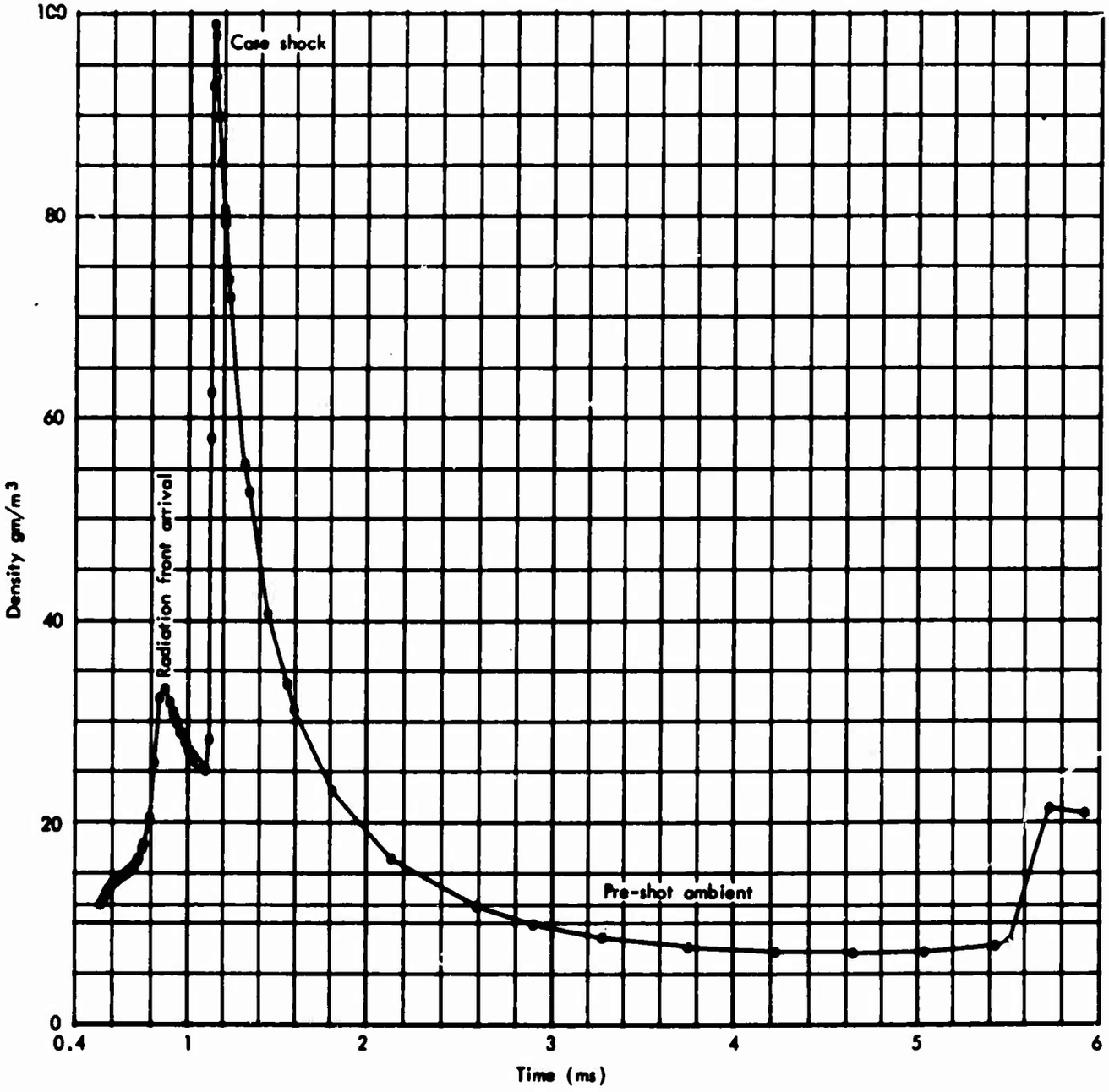

Fig. 2—Wall density versus time, 60 m radius, 1.7 KT

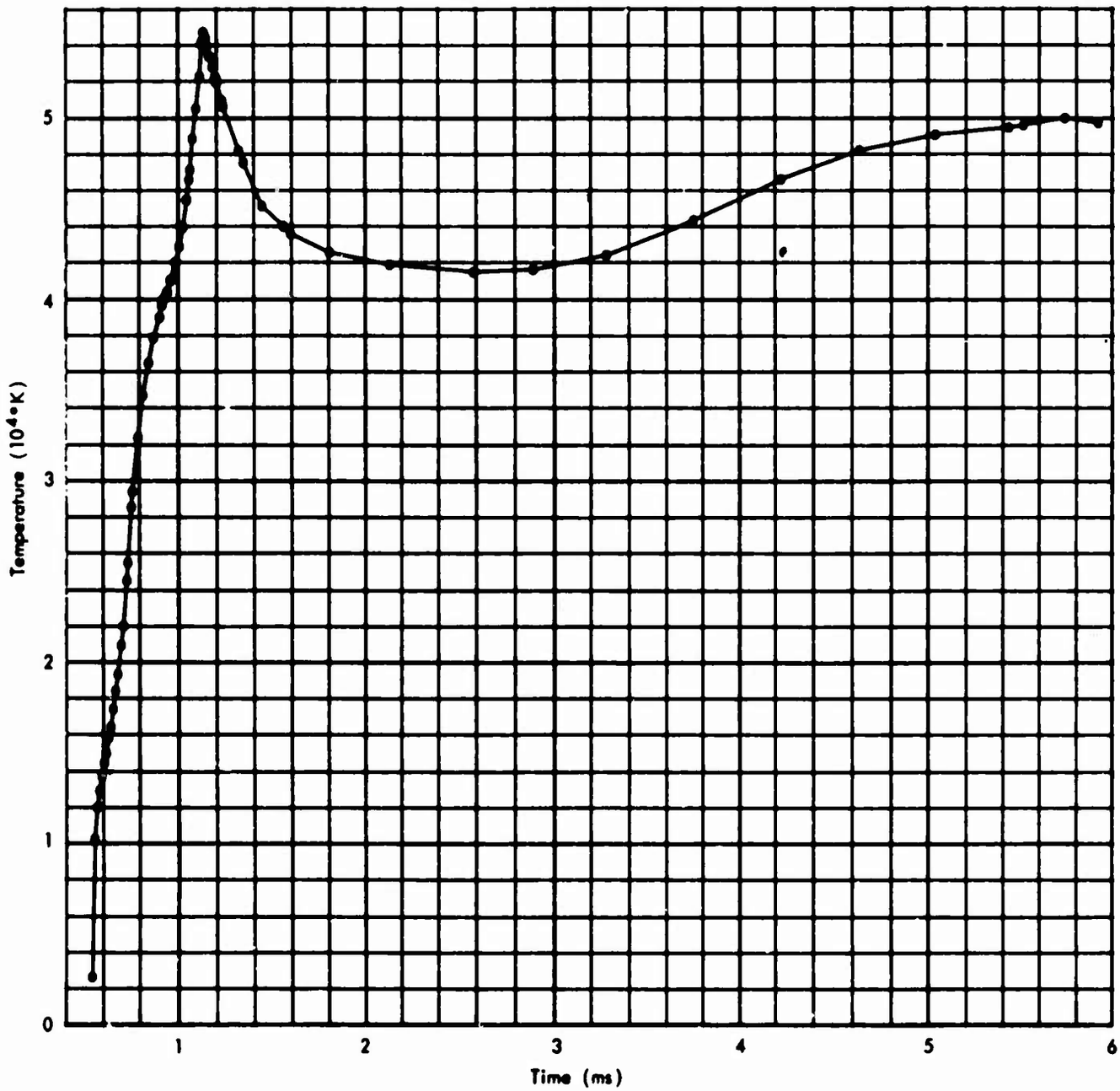

Fig. 3—Wall temperature versus time, 60 m radius, 1.7 KT

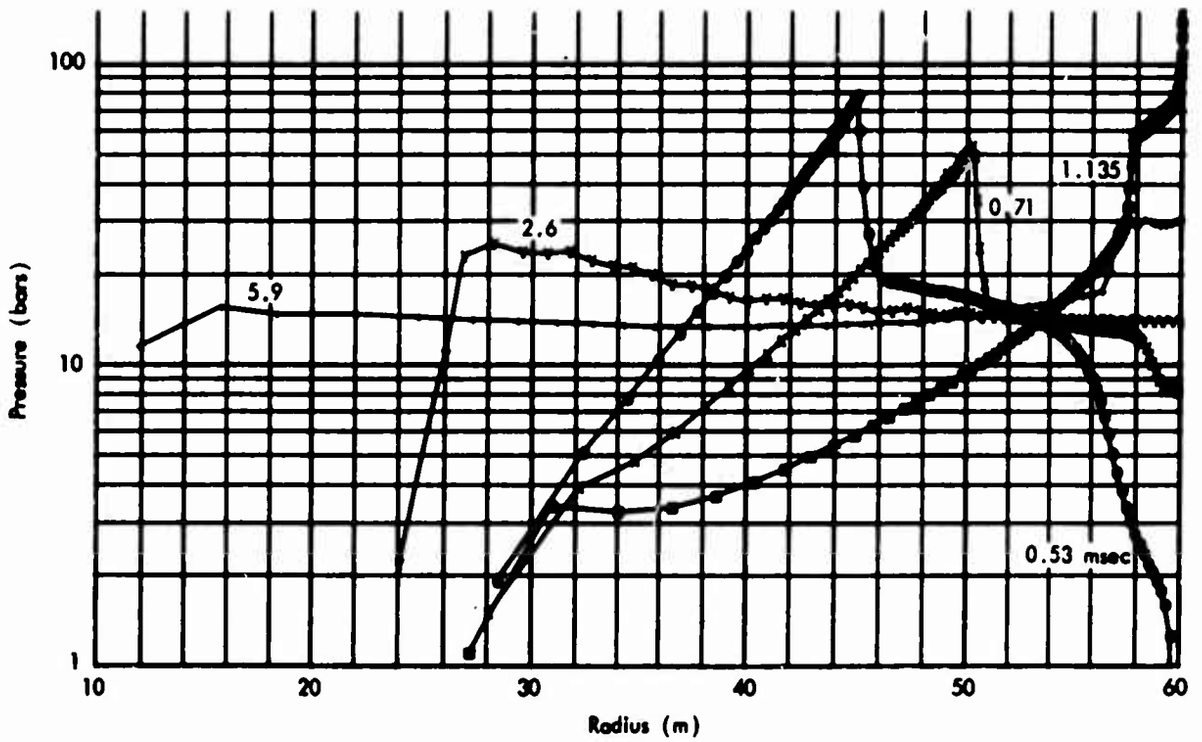

Fig. 4—Pressure profiles in 60 m cavity, 1.7 KT

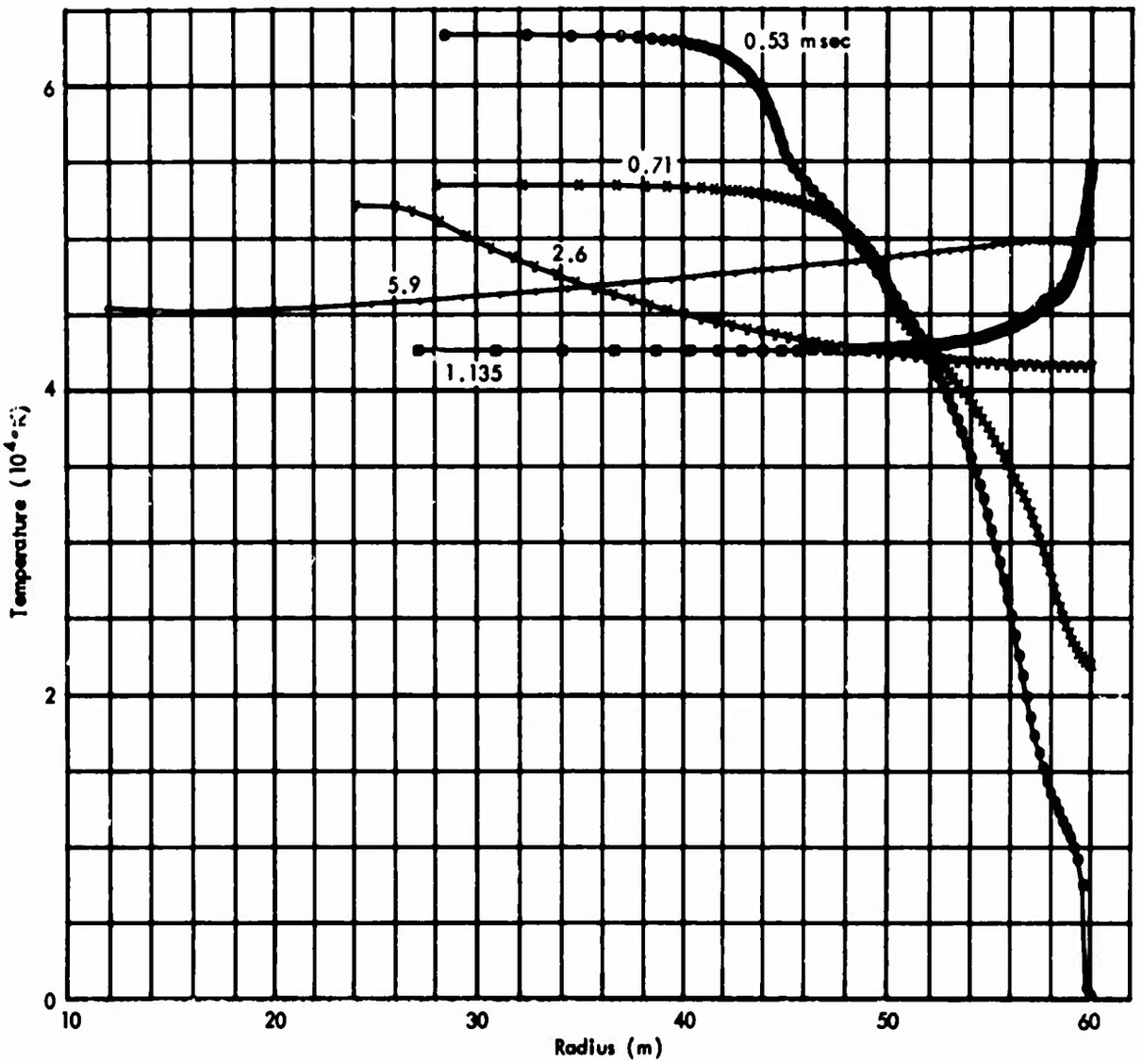

Fig. 5—Temperature profiles for 60 m cavity, 1.7 KT

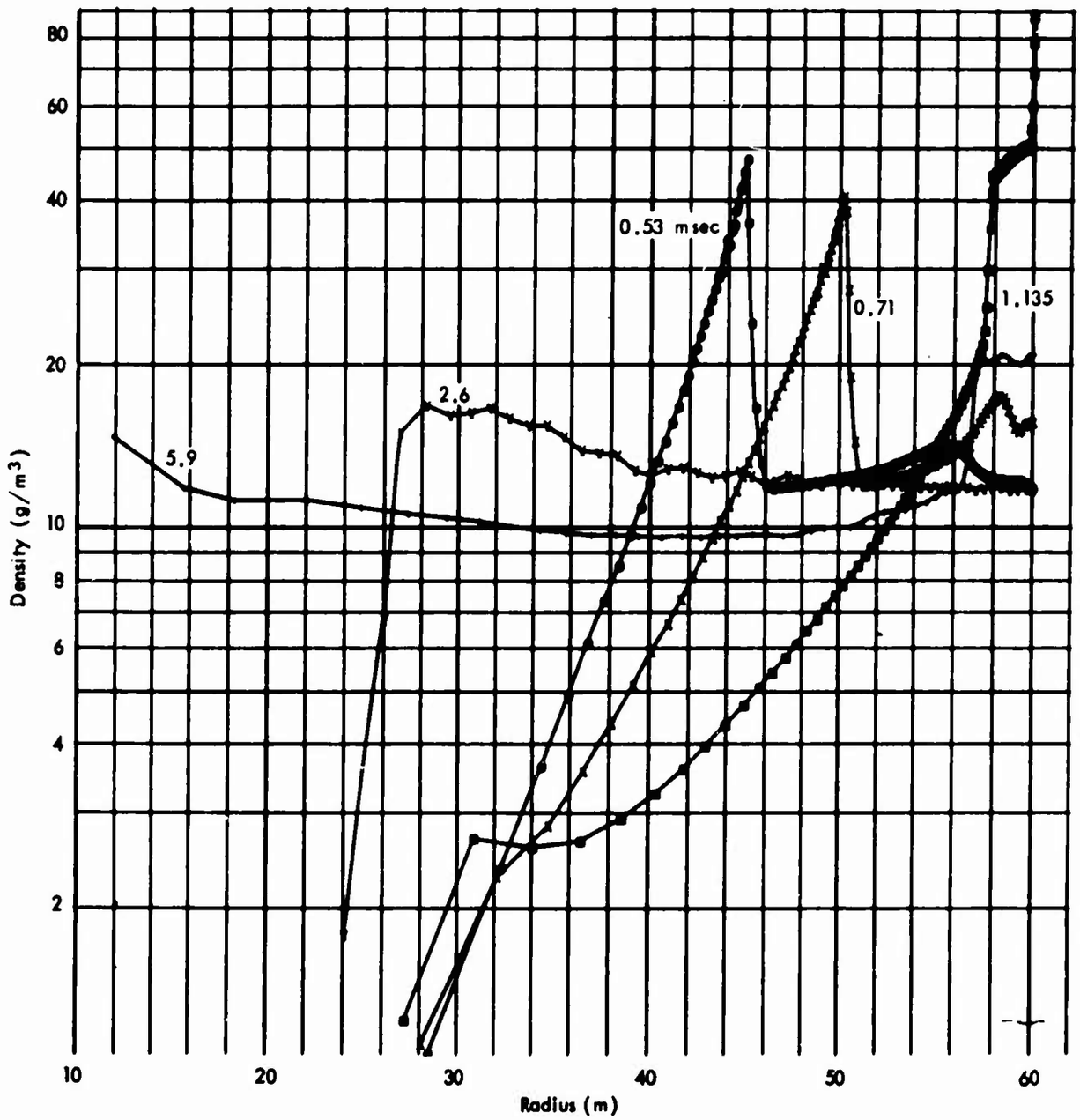

Fig. 6—Density profiles in 60 m cavity for 1.7 KT

for air (approximately the same as for water) was operative and had drained away a total of 69 tons of explosive energy (152.6 cal/cm^2 in the 60 m cavity). Since most of this energy is delivered to the walls by thermal radiation in a very short time, it is reasonable to assume that it penetrates less than a millimeter into the rock or other lining, and so is sufficient to raise the surface of the walls to vaporization temperatures. At that level, relatively opaque vapors should boil off the walls and little further energy (not contributing to the pressure) will leave the water vapor in the cavity, i.e., any further energy flow into the rock vapor should raise its temperature and pressure until such blow-off vapor is in equilibrium with the cavity gas.

THE EIGHTY METER CAVITY

For this large cavity radius, even for such low vapor pressures, the shock is well formed and has overtaken the radiation front long before reaching the wall. Consequently, the reflection at the wall is that of a strong adiabatic shock. The pressure, density, and temperature on the wall are shown in Figs. 7, 8, and 9 respectively for the rise and fall during the first reflection. Figure 10 shows pressure profiles before the shock reaches the wall. The earliest profile (.065 msec) displays a radiation front followed by the case shock. The subsequent profiles (.157, .36, and .89 msec) show the radiation front shocking up, but being overtaken by the case shock. By 1.68 msec, the two shocks have nearly merged into a single strong shock. The pressure profiles just before and after reflection are shown in Fig. 11.

Temperature profiles during the initial expansion are shown for the same times in Fig. 12. The early radiation front shows a considerable temperature gradient which is steepened as the shock forms. The low density interior behind the shocks becomes quite isothermal, but continues to decrease rapidly as the shocks and the now following radiation front expand further. Temperature profiles around the time of reflection are shown in Fig. 13.

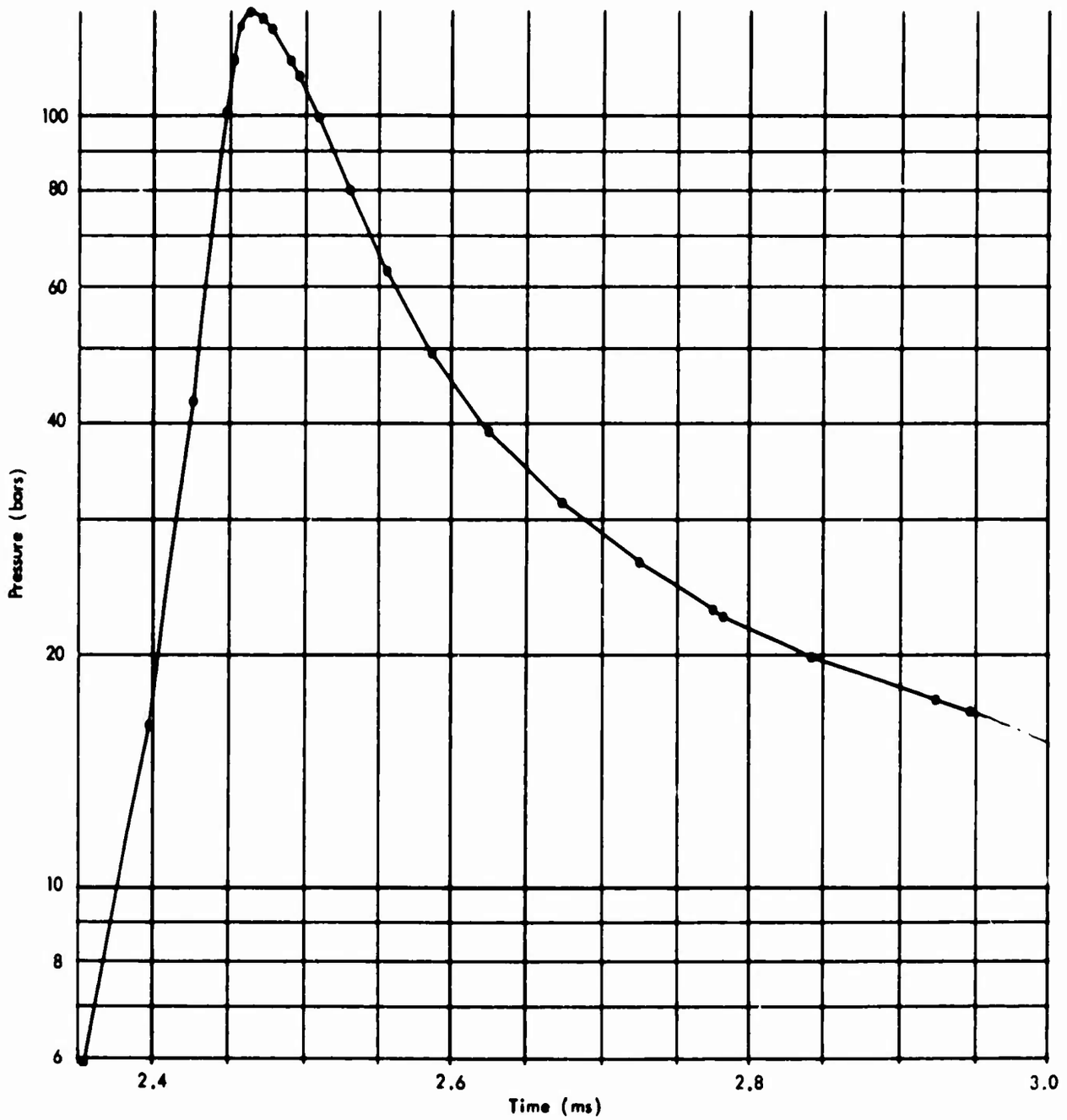

Fig. 7—Wall pressure versus time 80 m radius, 1.7 KT

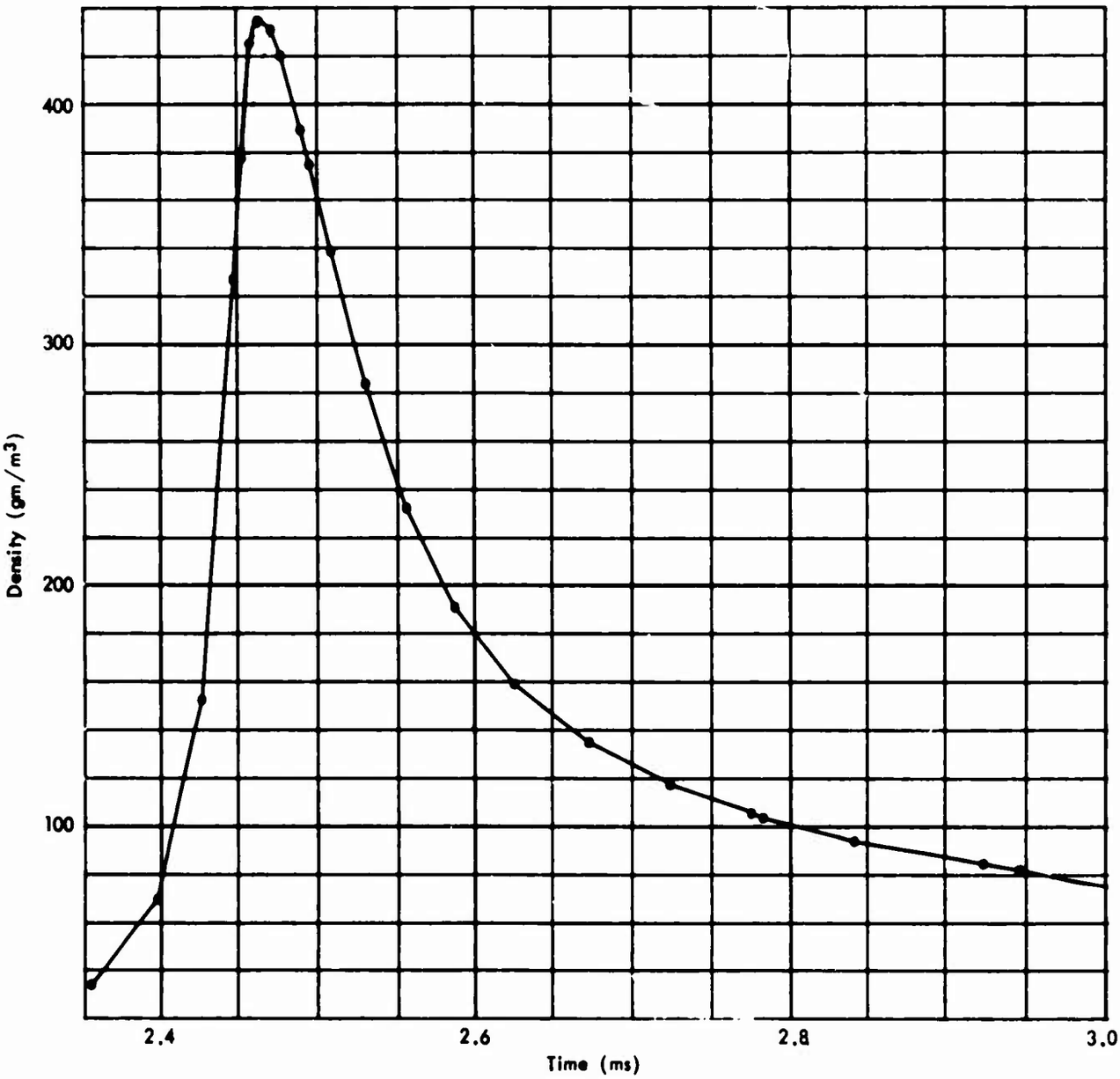

Fig. 8-- Wall density versus time 80 m radius, 1.7 KT

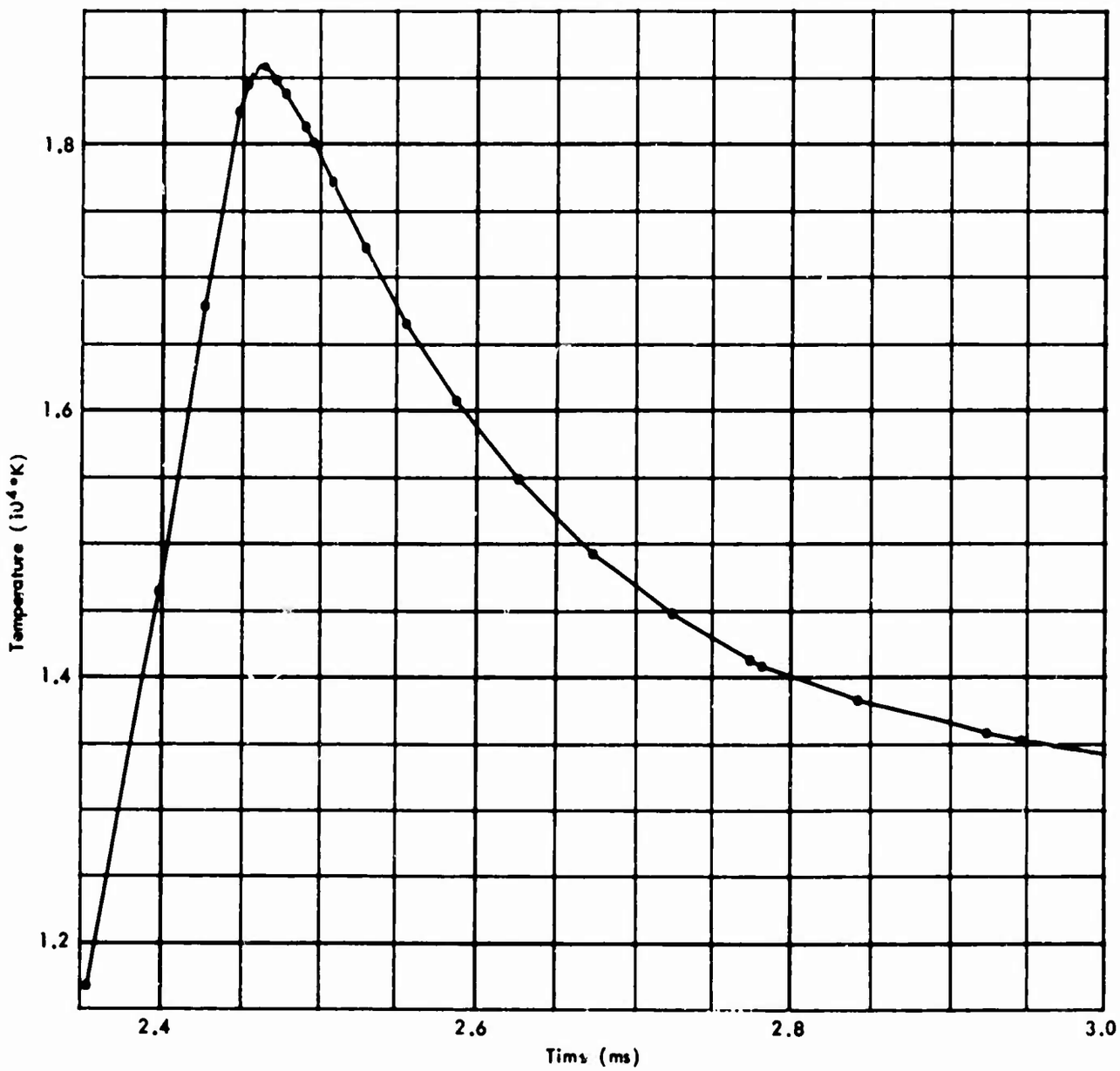

Fig. 9—Wall temperature versus time 80 m radius, 1.7 KT

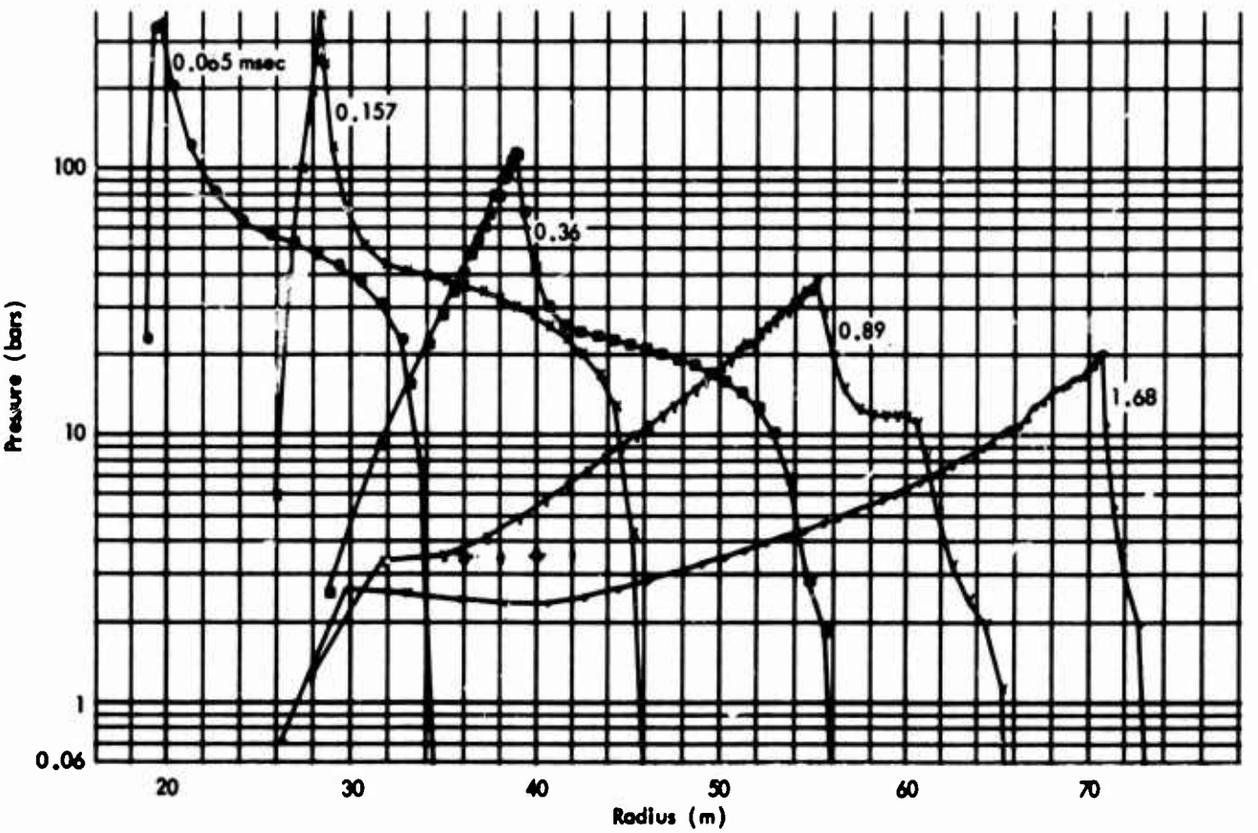

Fig. 10—Pressure profiles before first reflection, 80 m cavity, 1.7 KT

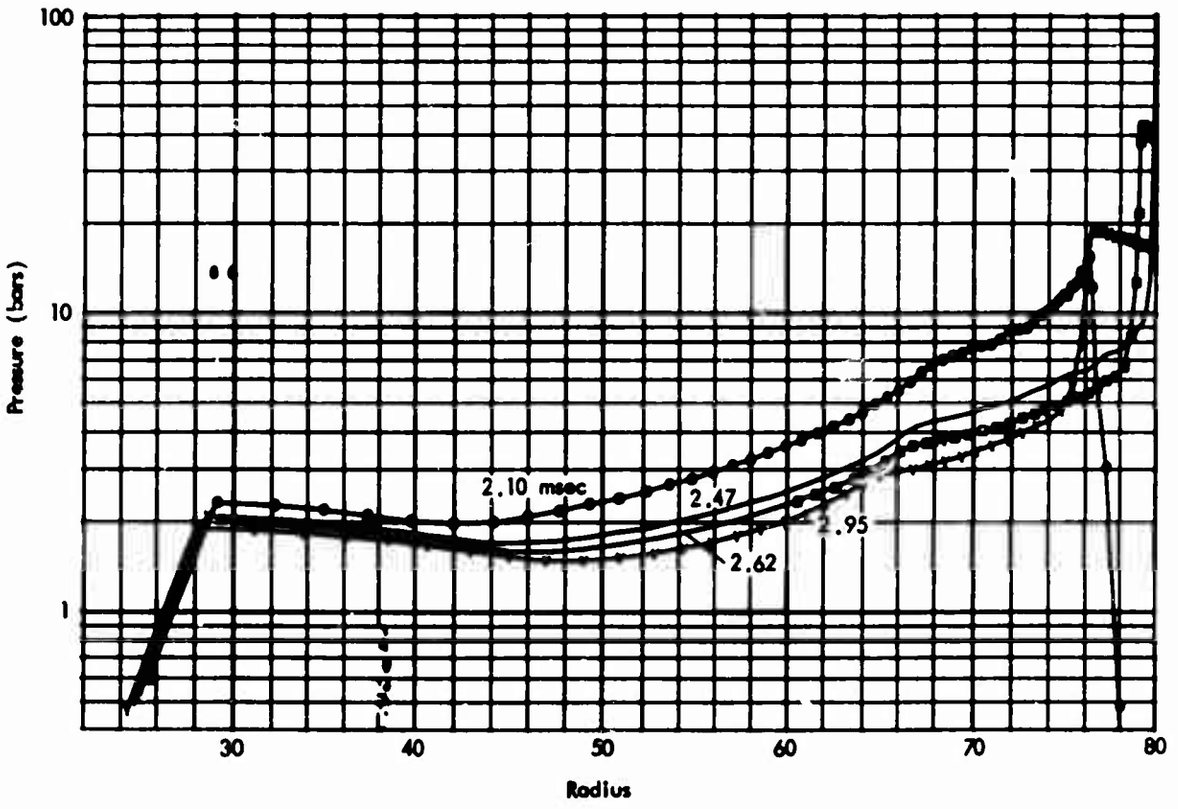

Fig. 11—Pressure profiles around time of wall reflection, 80 m cavity, 1.7 KT

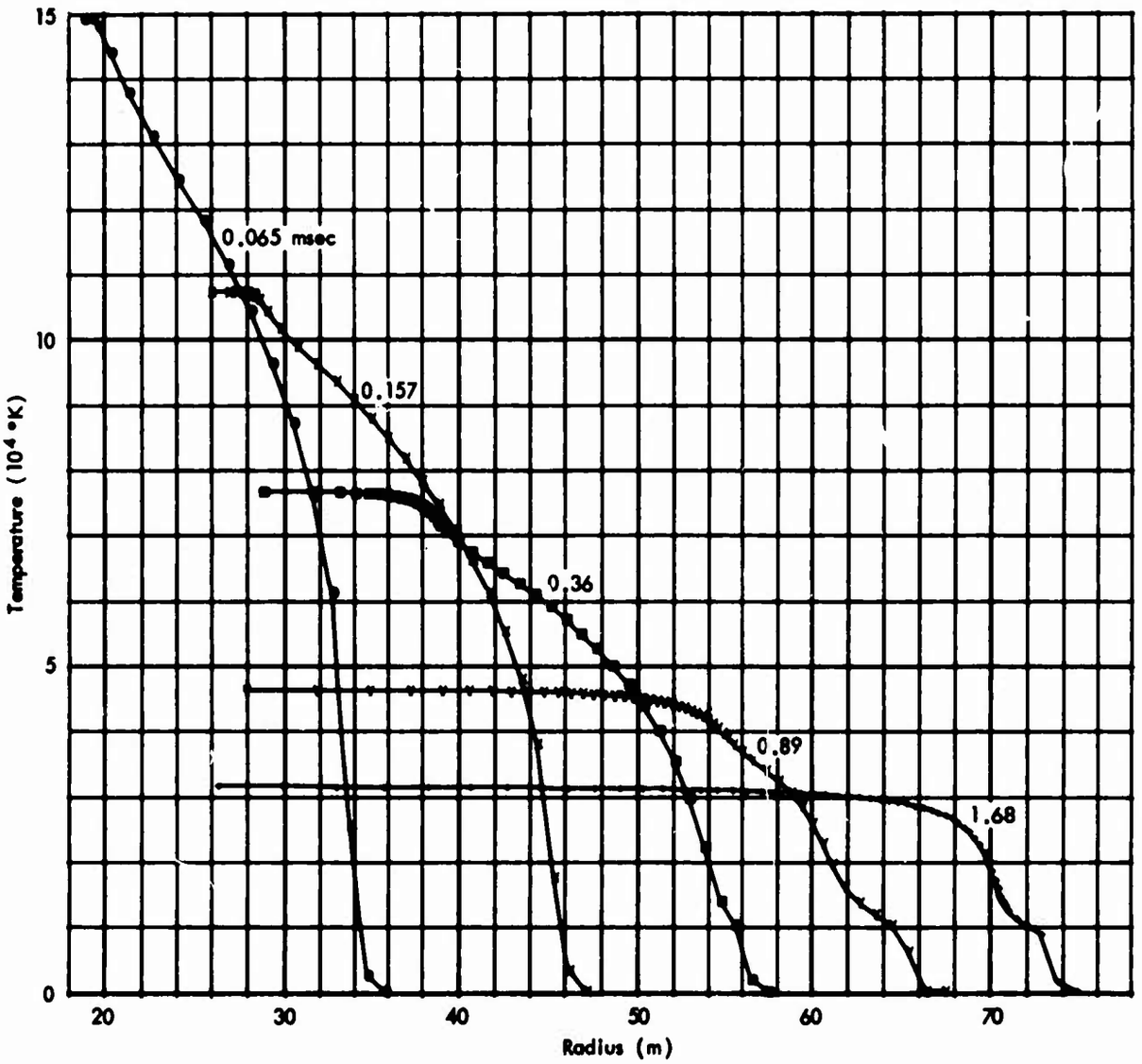

Fig. 12—Temperature profiles before first reflection, 80 m cavity, 1.7 KT

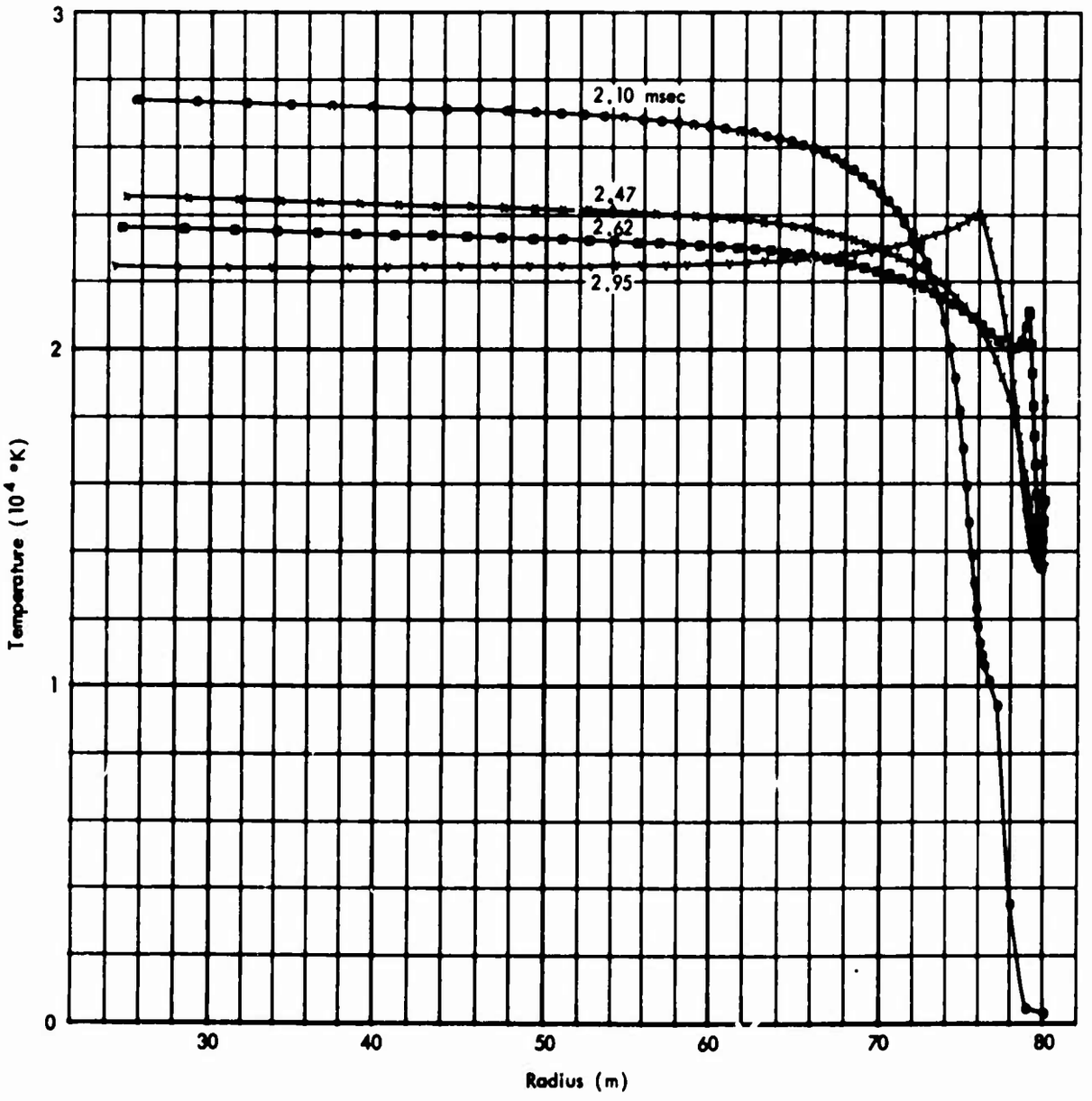

Fig. 13—Temperature profiles at times near reflection, 80 m cavity, 1.7 KT

The early density profiles (Fig. 14) show clearly the growth and the overtaking of the radiation front shock and the subsequent strong shock with nearly ten-fold compressions at the front. Reflection of this shock is shown in the density profiles of Fig. 15.

THE FORTY METER CAVITY

While the larger cavities (60 and 80 m) contain enough water vapor between the source and the walls to stop (or slow) the radiation and let a shock form, the smaller cavities -- in this case, 40 m radius -- allow radiation to reach the wall and raise the pressure to something like the average post-shot value before the case shock arrives. Figures 16, 17, and 18 show the wall pressure, density, and temperature for the case of 1.7 KT in a 40 m radius cavity. In each figure, the radiation wave shows some rise somewhat before the case shock arrival. The case shock drives the pressure to 676.5 bars (over an incident pressure of about 204 bars). The case shock at 40 m in a larger cavity, i.e., in the absence of a wall at 40 m, is only 120 bars. The difference ($\sim$ 84 bars) is due to the confinement (and reflection) of the radiation wave. In the absence of a cavity wall, the pressure maximum at 40 m in the passing radiation driven wave is 29.1 bars, the temperature 72,200 ^{o}K. The influence of the wall is to confine the energy and allow it to equalize throughout the cavity so that the temperature is very quickly made nearly constant at around 10 or 11 electron volts (ev). This not only raises the temperature at the wall above that which would exist at 40 meters from the same burst in a larger cavity, but boosts the pressure also.

Figure 19 illustrates the effect on pressure profiles of the rapid thermal equalization in the cavity caused by the radiation transport. The earliest profile shown in Fig. 19 (.10 msec) is just before the radiation wave reaches the wall, so a steep gradient in temperature and pressure exists near the wall (40 m). At reflection (.40 msec), the wall pressure spikes up, but thereafter drops as the shock returns toward the origin. The corresponding temperature profiles (Fig. 20) show even more dramatically the dominance of

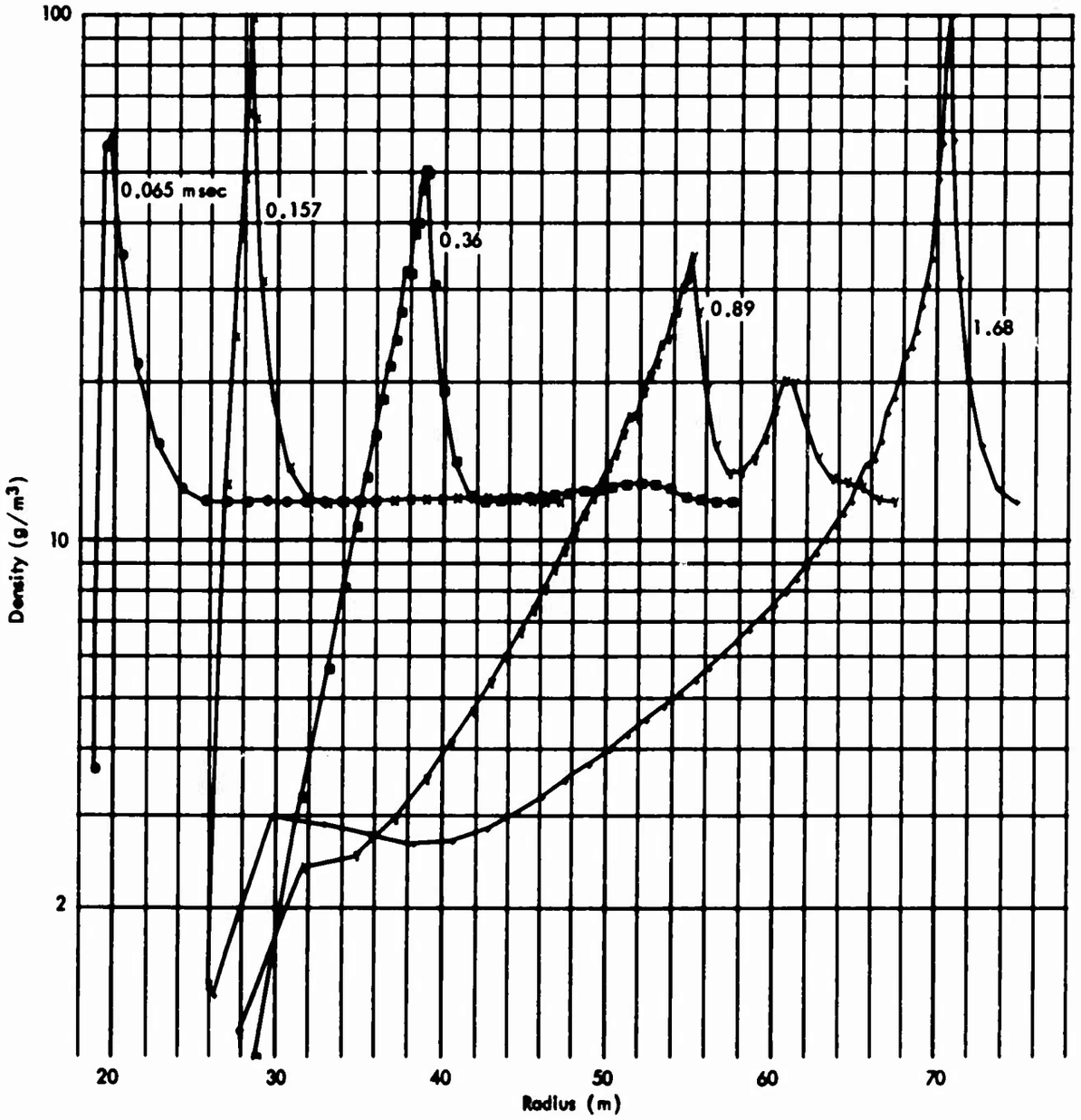

Fig. 14—Density profiles before first reflection, 80 m cavity, 1.7 KT

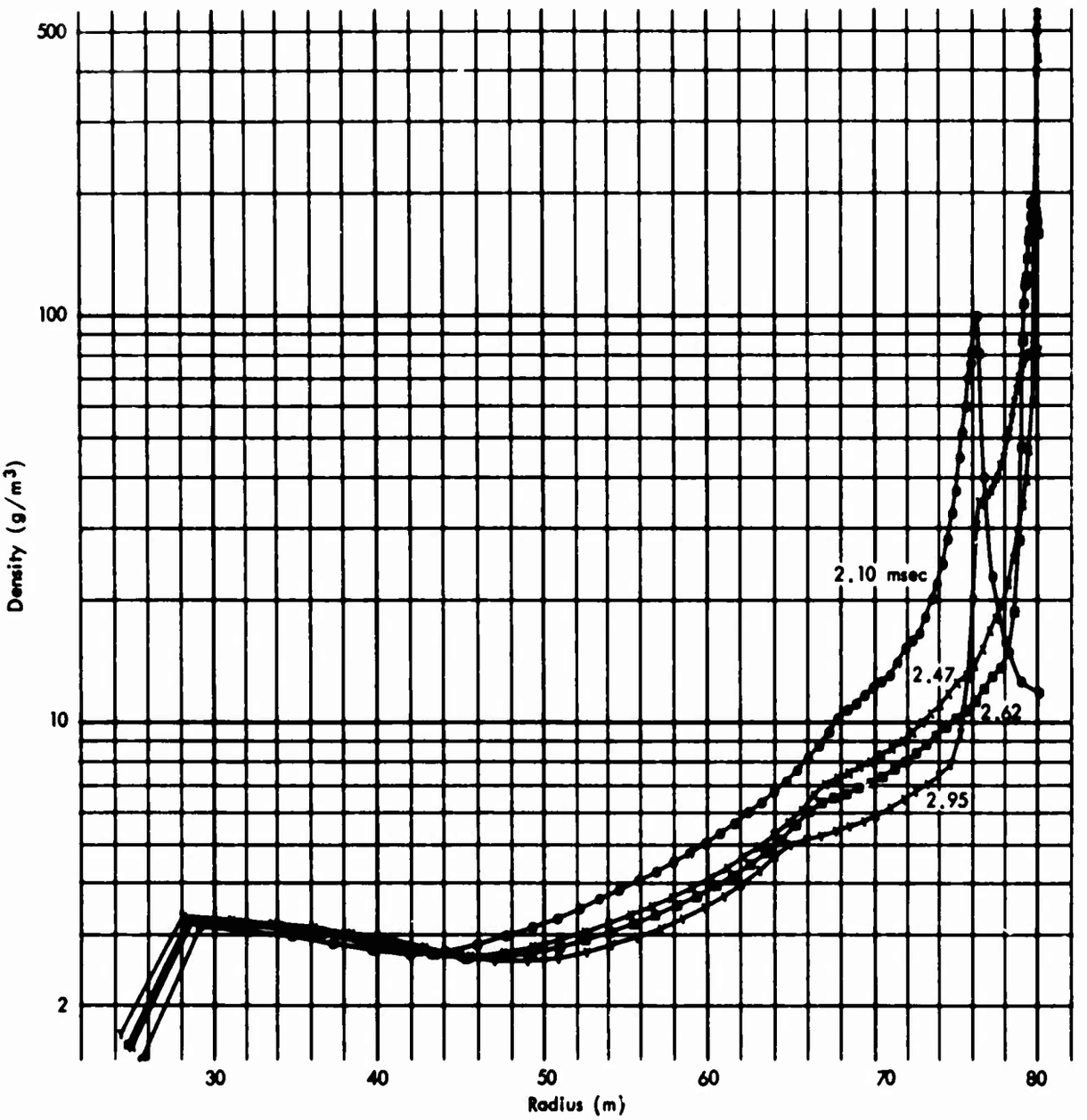

Fig. 15—Density profiles at times near wall reflection, 80 m cavity, 1.7 KT

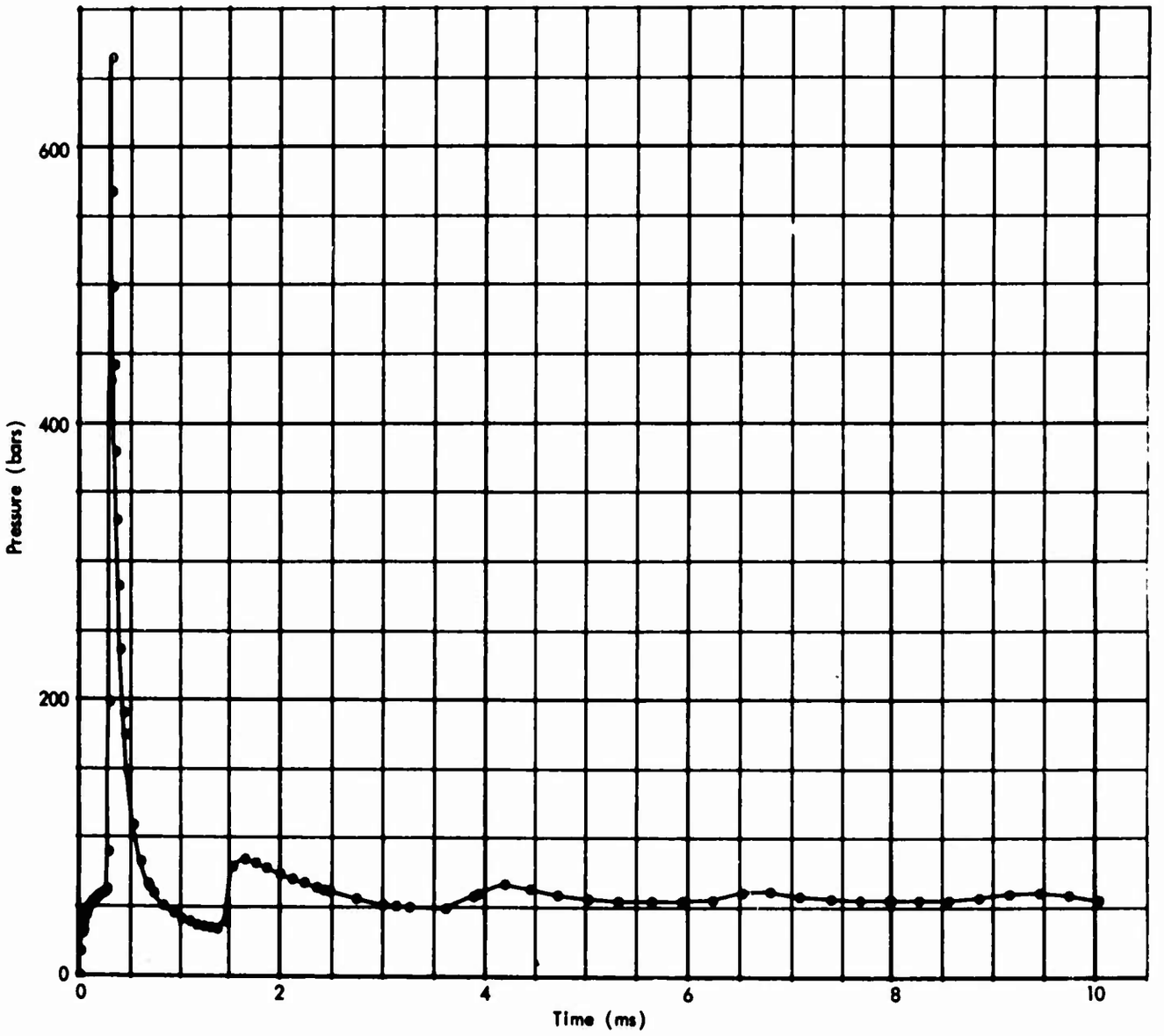

Fig. 16—Wall pressure versus time, 40 m cavity, 1.7 KT

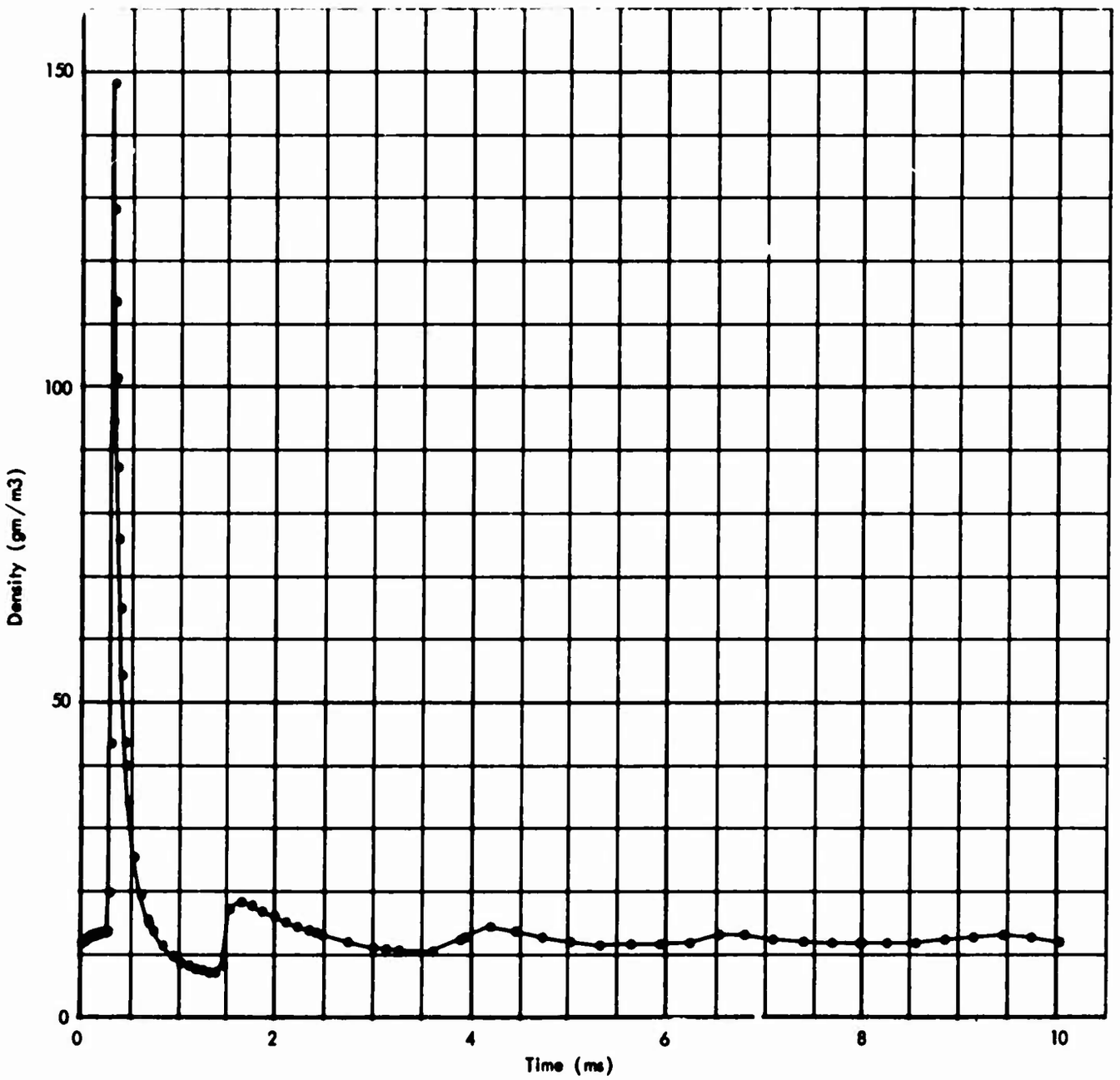

Fig. 17—Gas density at wall versus time, 40 m cavity, 1.7 KT

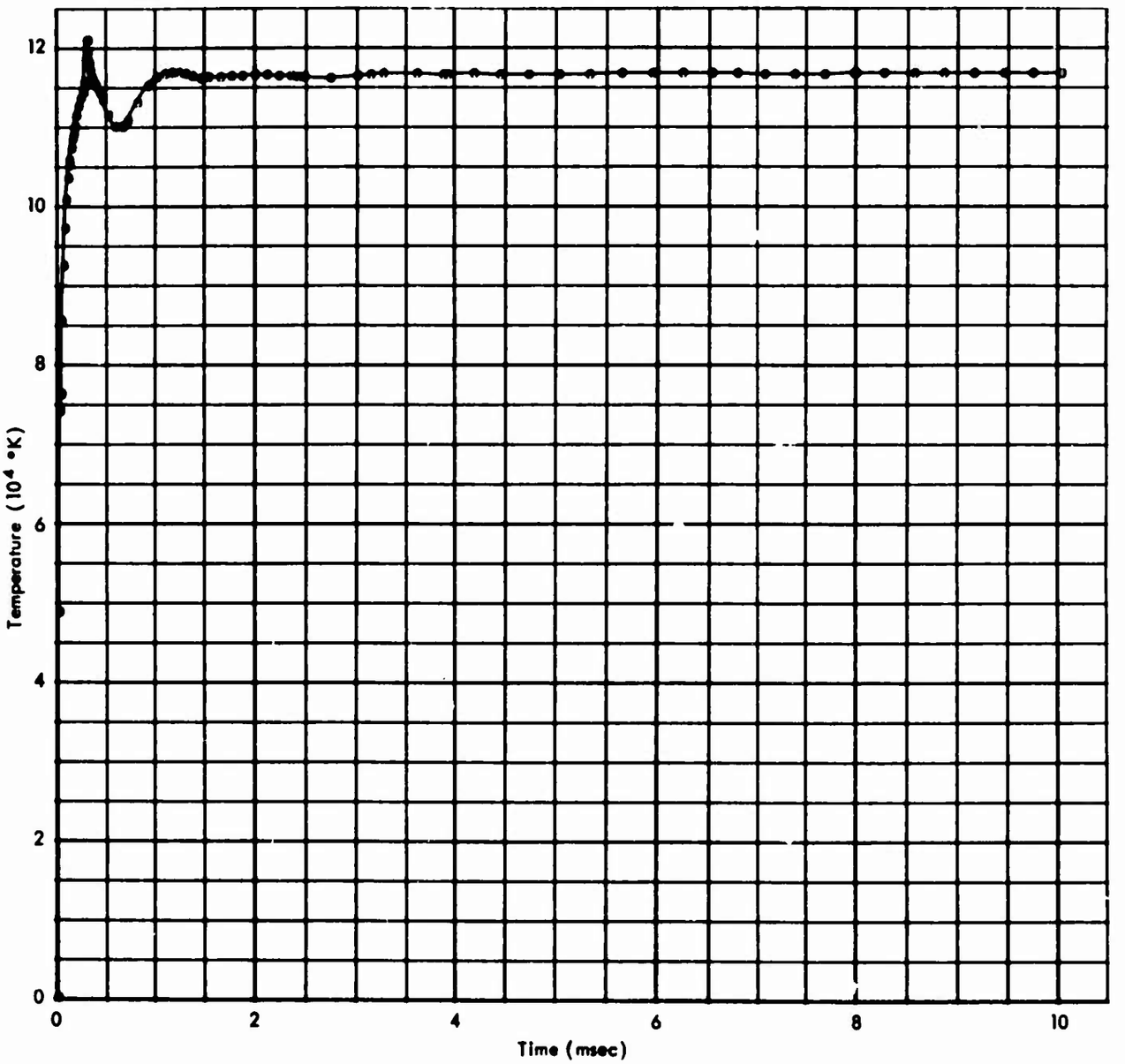

Fig. 18—Gas temperature at wall, 40 m cavity, 1.7 KT

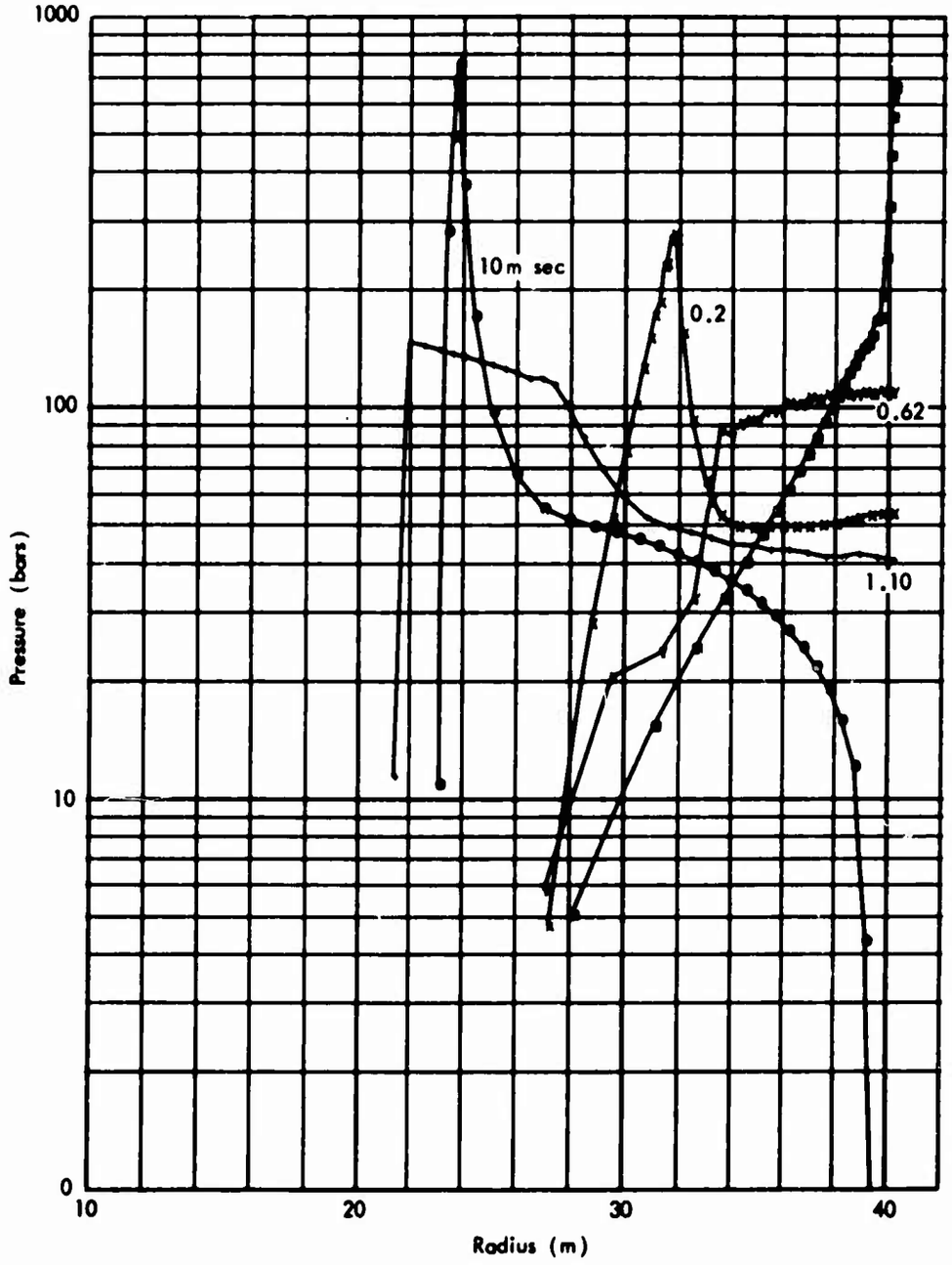

Fig. 19—Pressure profiles before and after reflection, 40 m, 1.7 KT

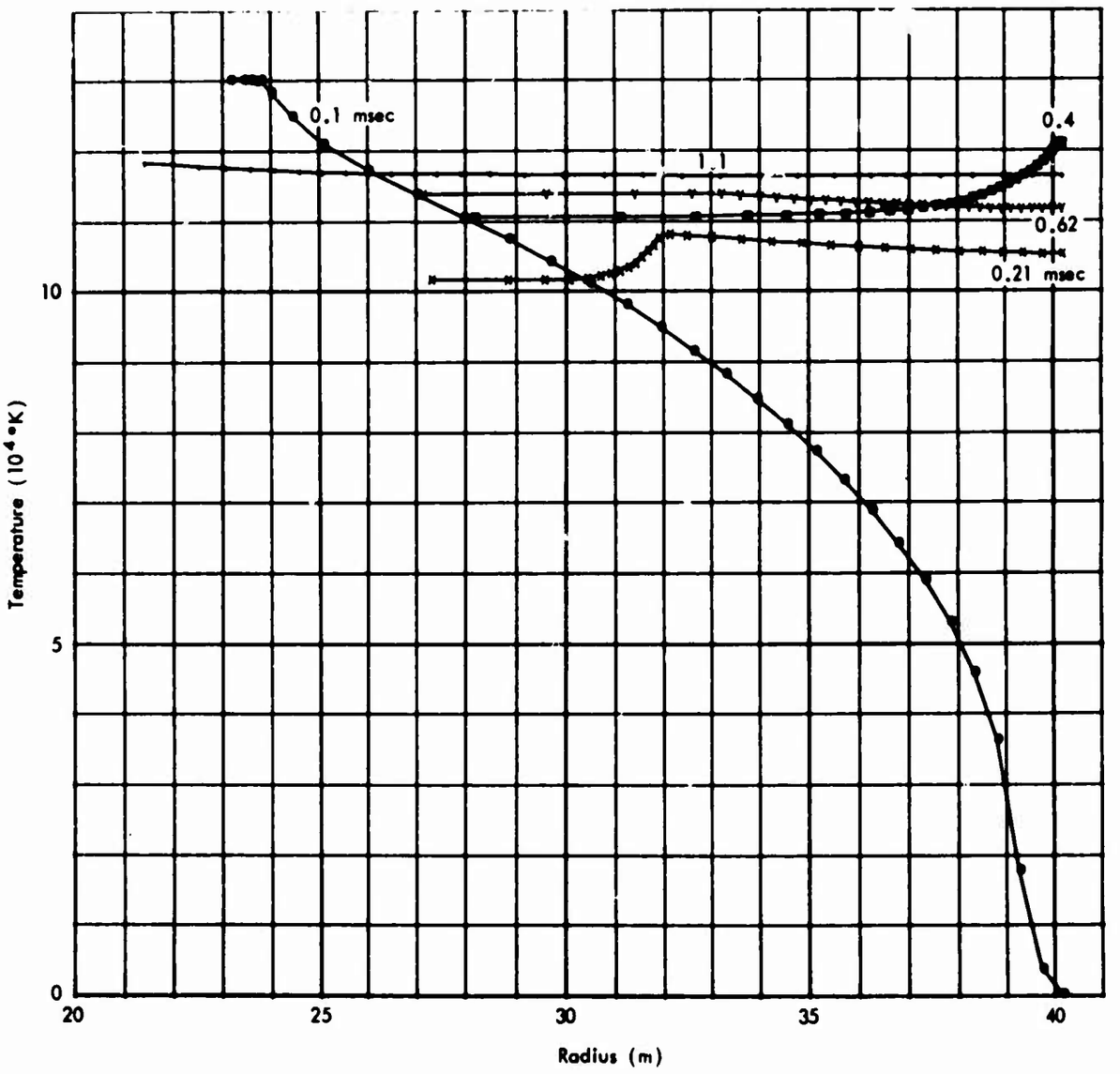

Fig. 20—Temperature profiles, 40 m cavity, 1.7 KT

radiation in destroying all temperature gradients even while shock waves continue to traverse the cavity. The density profiles of Fig. 21, at the same times, show the case shock behind the radiation-driven wave before either reach the wall (.10 msec), and the accumulation of nearly all the mass near the wall at the peak reflection (.40 msec). The velocity profiles at these times (Fig. 22) show the shock reflection and subsidence of motion in the cavity.

This problem (40 m cavity radius, 1.7 KT) was treated as isothermal hydrodynamics after 8 msec, very much simplifying the calculation. Since the temperature by that time was the same in all zones to at least four significant figures, and all mfp's were long, no further temperature changes could be expected and radiation transport would serve only to perpetuate that isothermal state in a complicated way. Hydrodynamics alone was then permitted with no change in temperature allowed, i.e., pressure was a function of density alone and the energy was no longer computed in each zone. (It, too, was unchanged.) The results computed both with and without detailed radiation diffusion were quite the same after many cycles, but the simple isothermal calculation runs much faster and was used to extend the calculation to beyond 40 msec.

The late time wall pressures and densities are shown in Figs. 23 and 24. A slight blip at 8 msec indicates the effect of the change to isothermal hydrodynamics. The late time oscillations show a frequency of about 275 cps (3.63 msec/cycle), and an amplitude of peak pressure decay proportional to about the inverse cube of the time.

SIXTY METER CAVITY WITH TEN KILOTONS

The several times higher yield in the same source mass and cavity atmosphere results in a much hotter cavity dynamics, dominated from the outset by radiation. Whereas the basic source (1.7 KT) produced a radiation wave by doing work on the surrounding atmosphere (not at all by radiation diffusing out of the source), when the yield is raised to 10 KT in the same mass, slightly more than two thirds of the energy comes out as radiation. In the latter

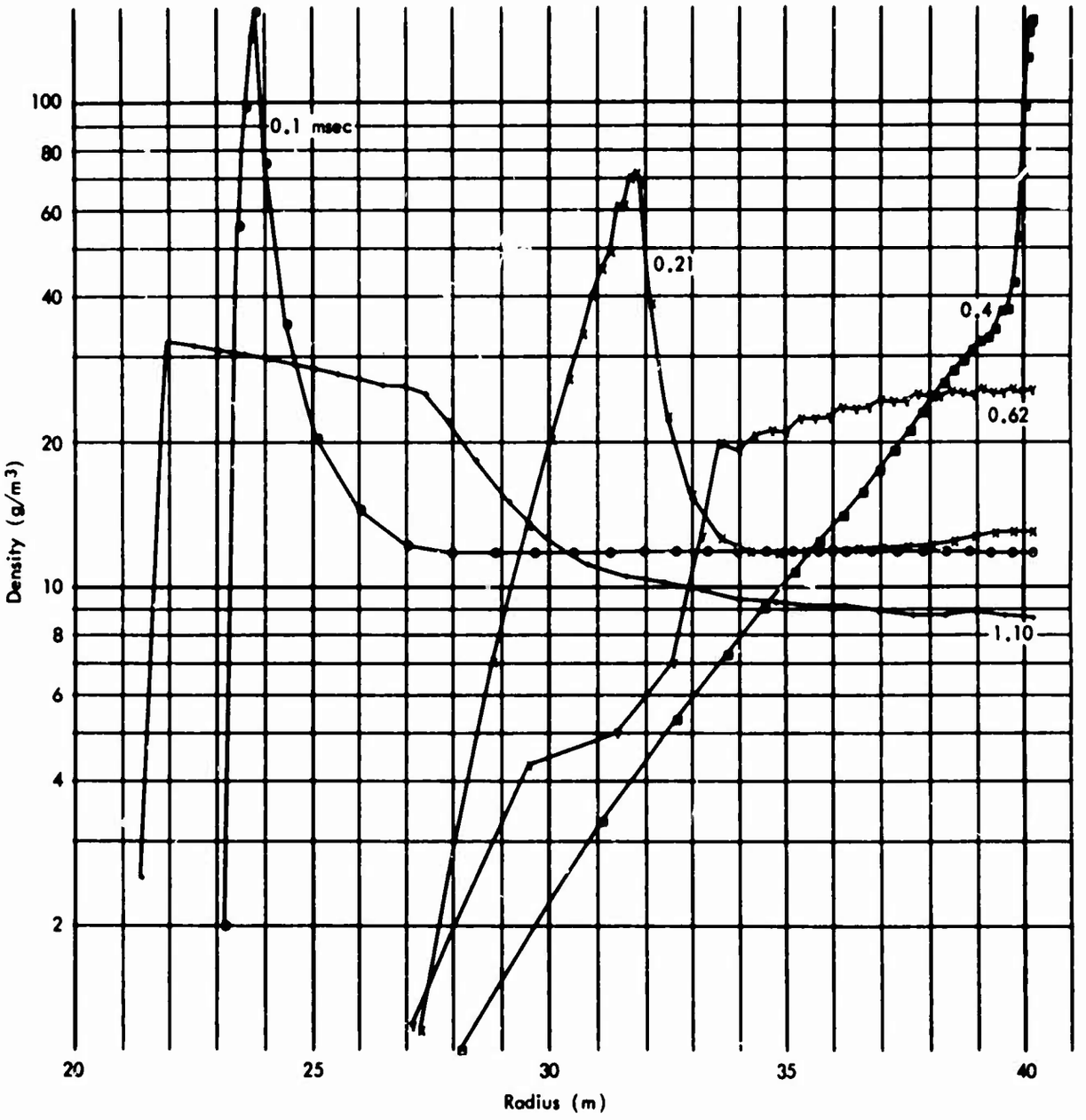

Fig. 21—Density profiles, 40 m cavity, 1.7 KT

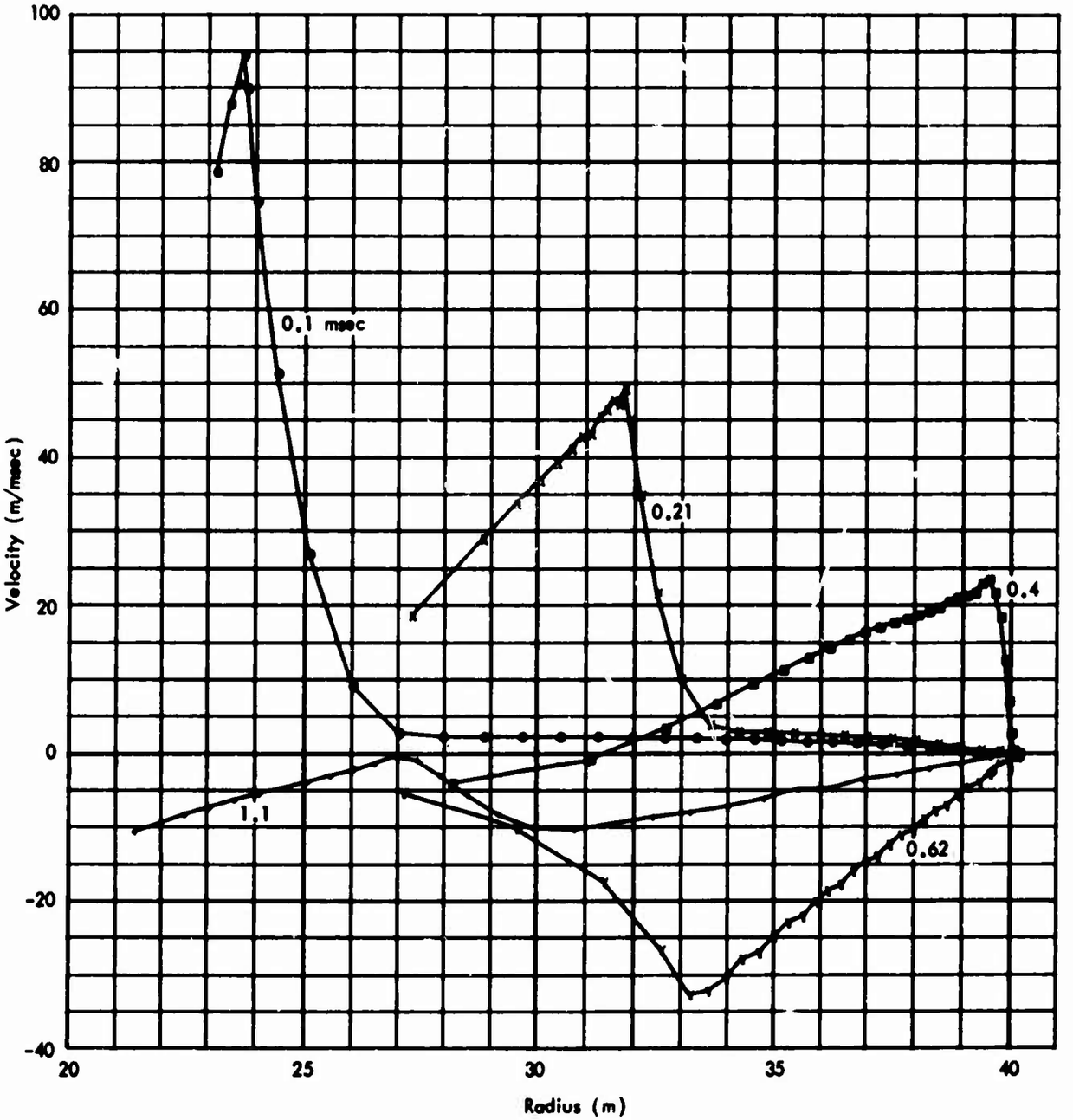

Fig. 22—Velocity profiles, 40 m cavity, 1.7 KT

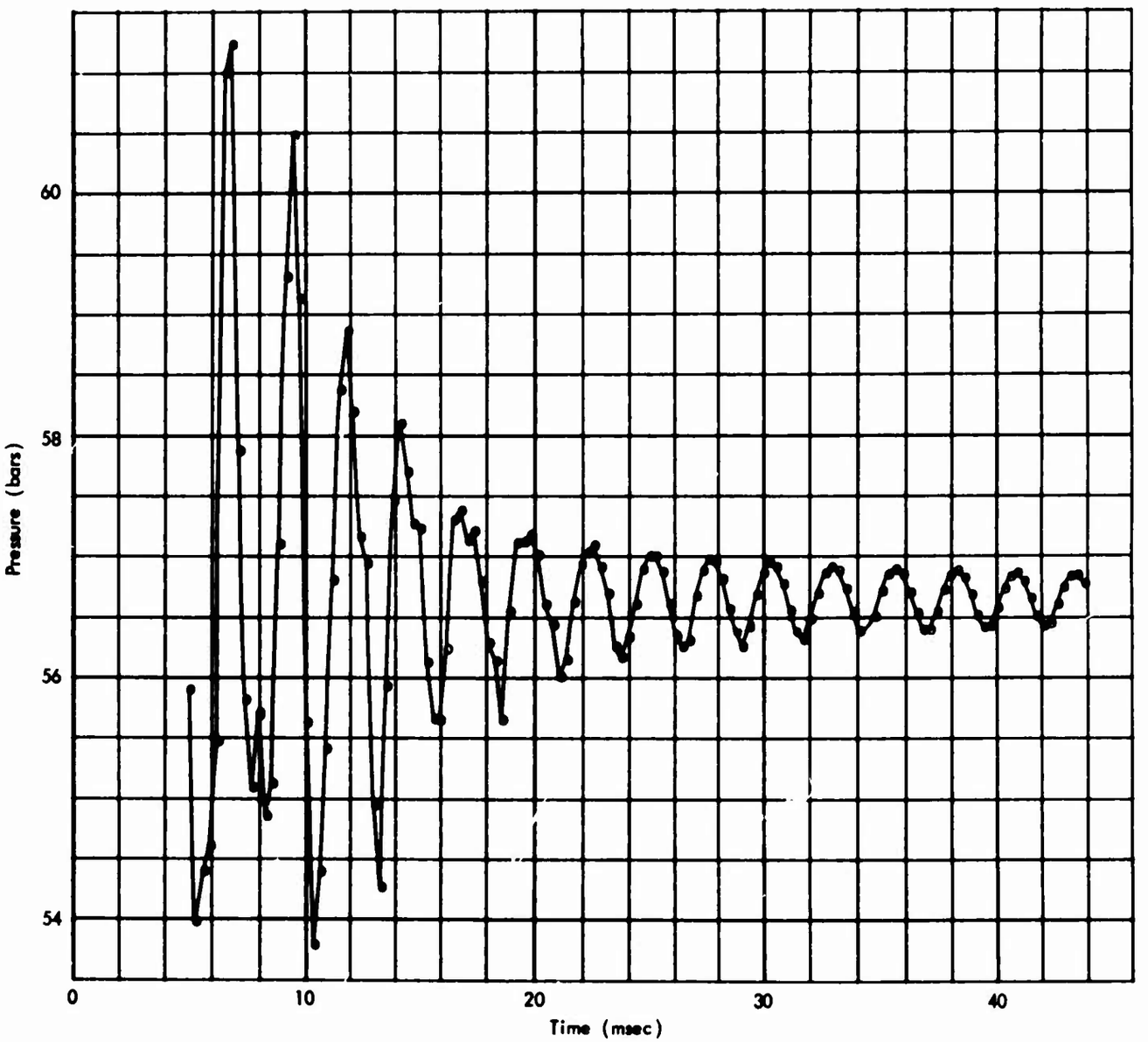

Fig. 23—Late wall pressure versus time, 40 m cavity, 1.7 KT

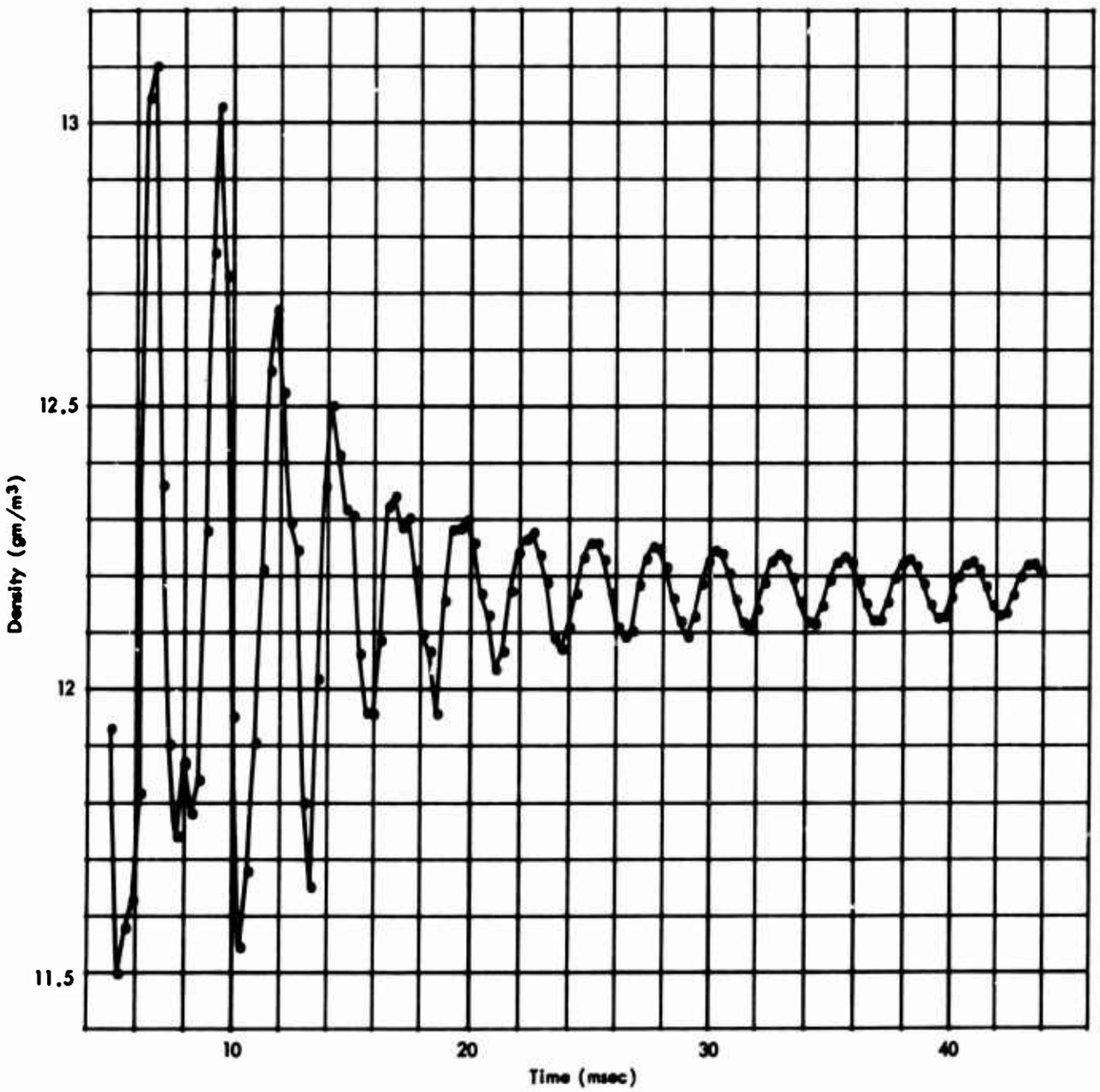

Fig. 24—Late density at wall versus time, 40 m cavity, 1.7 KT

case, the flood of radiation quickly isothermalizes the cavity, so that the simpler isothermal calculation was possible after about 0.2 msec, and long before the case shock reached the wall. Figure 25 shows wall pressure versus time for the 10 KT case. The radiation drives the pressure to 92.3 bars, the case shock runs it up to a spike at 382.8 bars, with a second reflection 2.35 msecs later reaching only 141 bars.

The wall density-time history is shown in Fig. 26, and is similar to the pressure history. The temperature, however is quite uninteresting, since it rises in a fraction of a millisecond to 16.94 ev and then remains constant. Figure 27 shows pressure profiles before and at first reflection. Because of the strong radiative phase preceding the case shock, an appreciable pressure ($\sim$ 90 bars) exists in front of the shock, and the shock is neither strong nor adiabatic. The later pressure profiles, after the first reflection are illustrated in Fig. 28. Corresponding density profiles are shown in Figs. 29 and 30, and velocity profiles are given for the same times in Figs. 31 and 32. Note the strong negative phase following the initial outward shock in Fig. 31, and note the strong reflected shock in Fig. 32.

FORTY METER CAVITY - HALF MASS SOURCE

To briefly investigate the influence of the mass associated with the nuclear explosion source, a separate calculation was run identical to the earlier 40 m cavity problem but with one half the mass of aluminum in the source. This is a significant difference, since in the half-mass case, nearly 24% of the yield is driven into the water vapor by radiative diffusion, while in the whole-mass case, energy gets into the water vapor as work is done by the expanding aluminum. The plot of wall pressure versus time for this variation (Fig. 33) shows that the radiative phase is enhanced and the case shock weakened as might be expected. The peak wall reflection of the case shock runs to only 350 bars, while the original problem rose to 676.5. The gas density at the wall is shown to rise to 80 gm/m^3 in Fig. 34. The gas temperature at

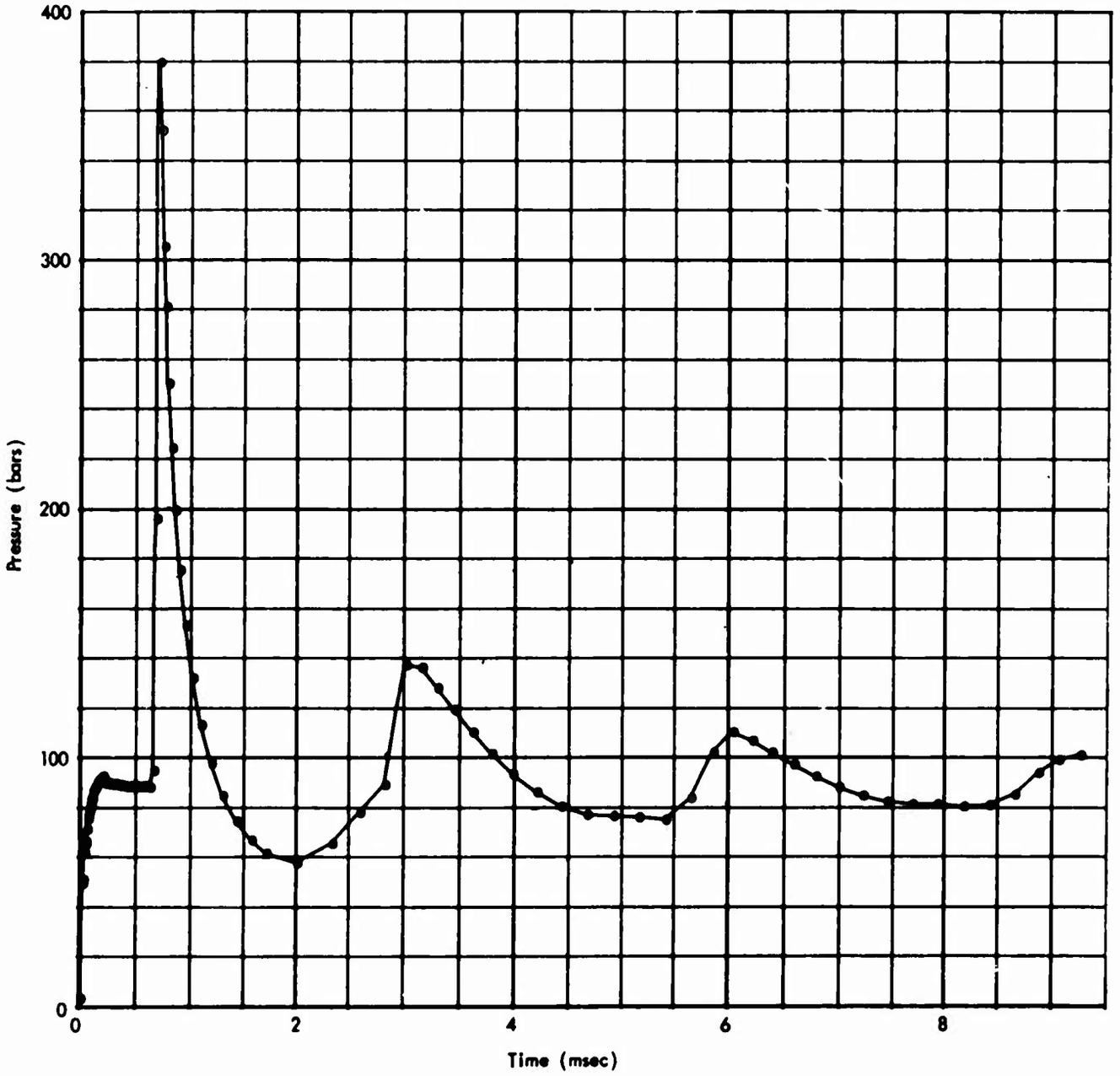

Fig. 25—Wall pressure versus time, 60 m cavity, 10 KT

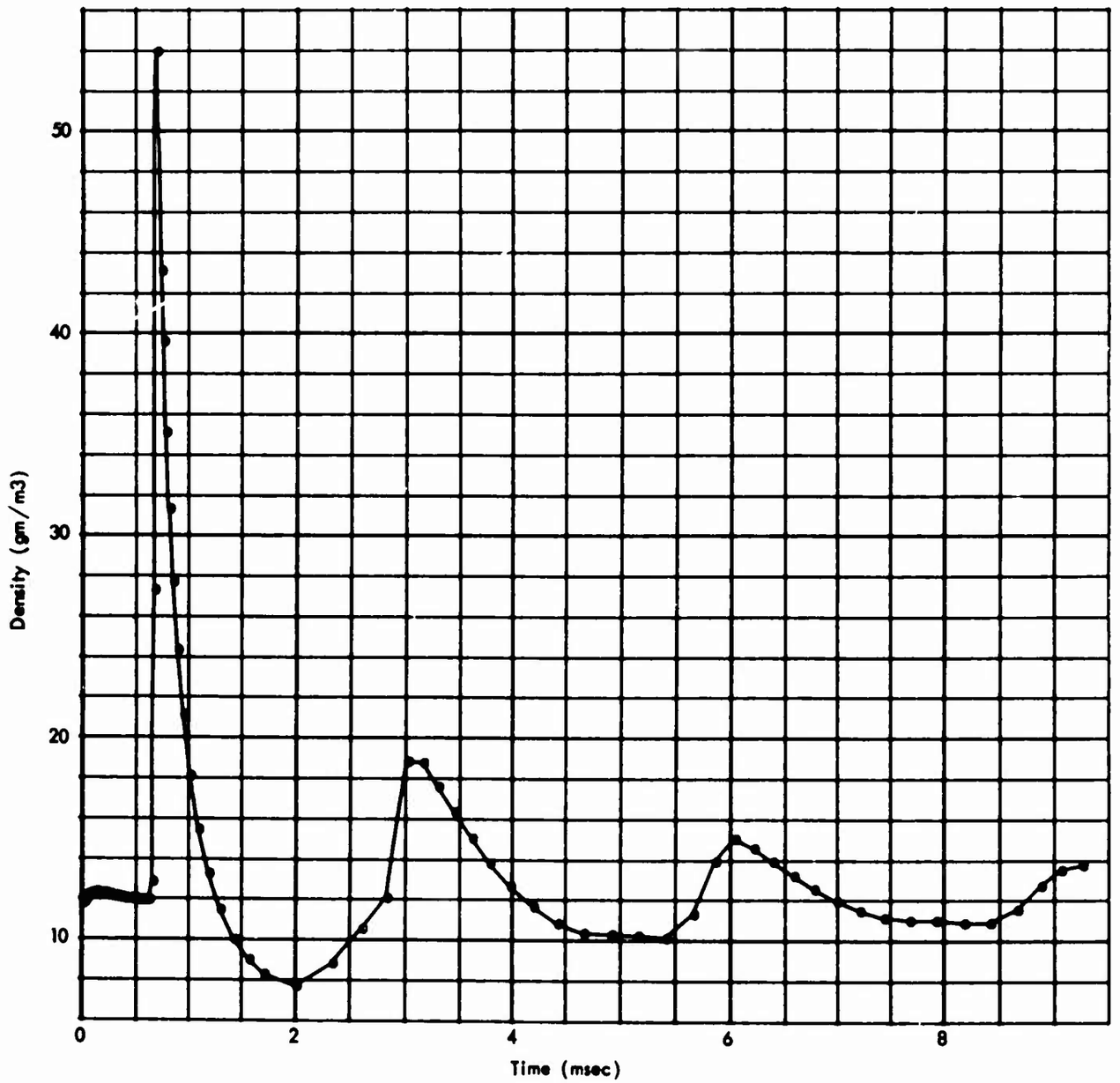

Fig. 26—Gas density at wall versus time, 60 m cavity, 10 KT

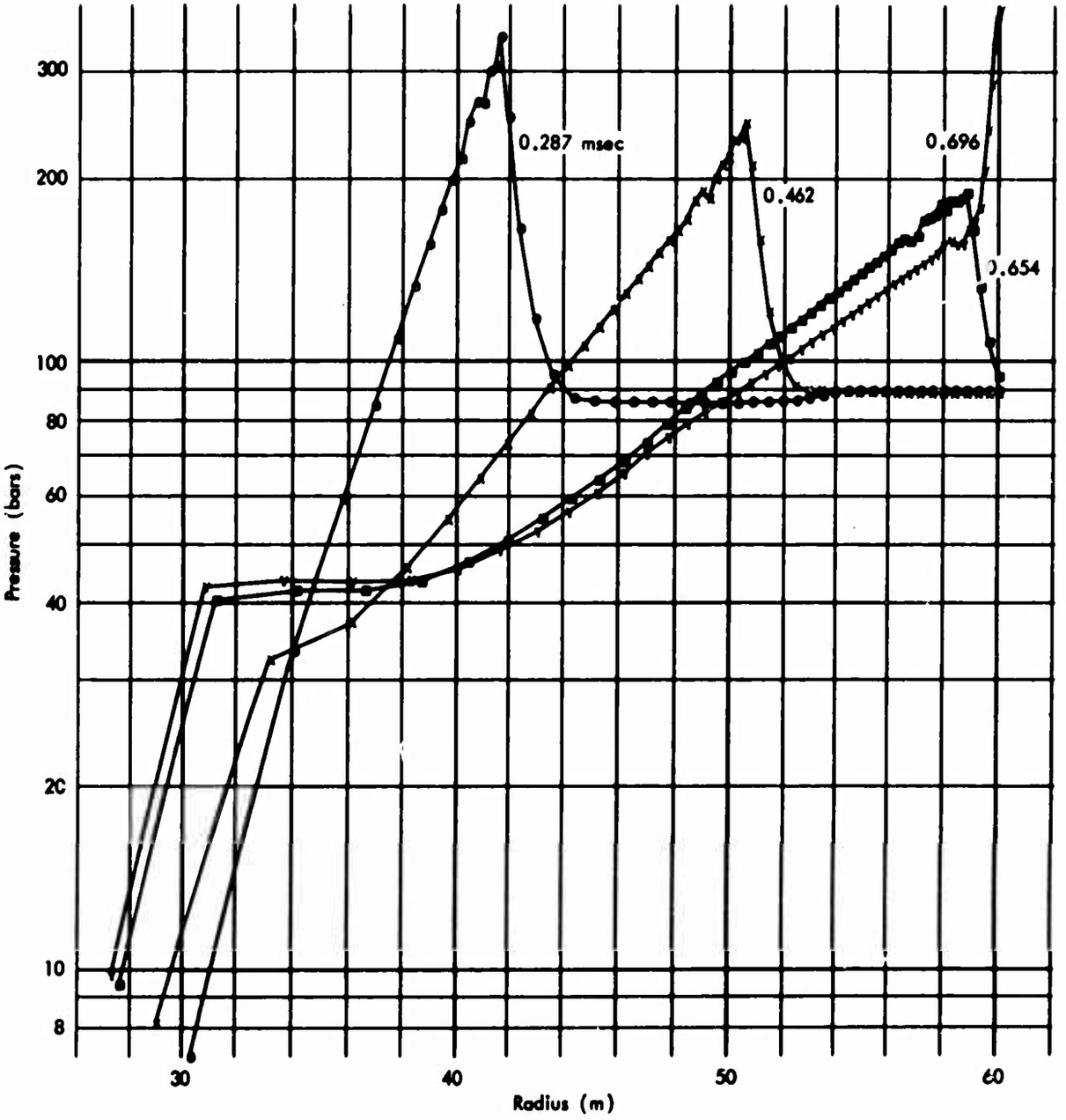

Fig. 27—Early pressure profiles, 60 m, 10 KT

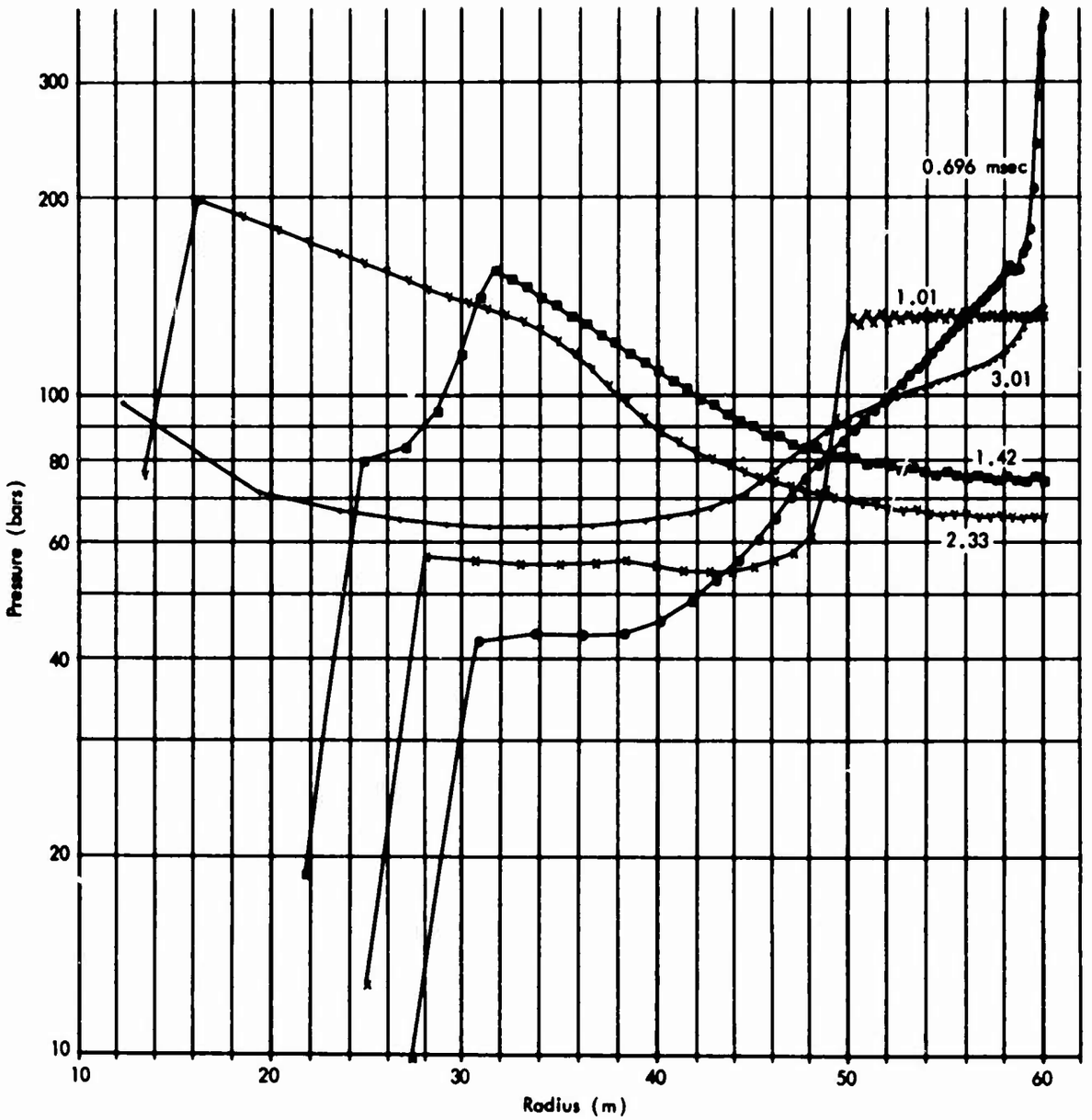

Fig. 28—Pressure profiles after first reflection, 60 m, 10 KT

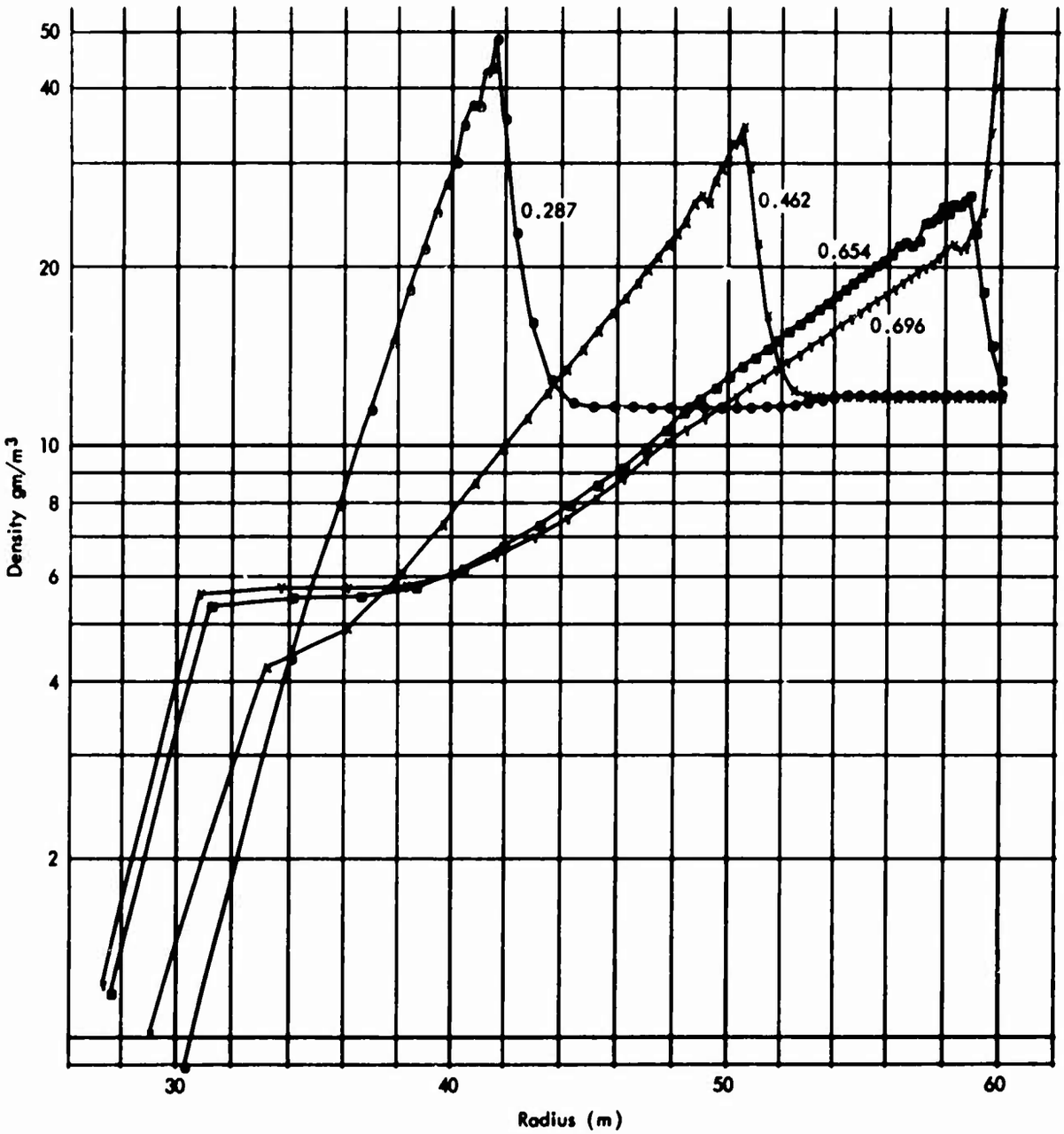

Fig. 29—Early density profiles, 60 m, 10 KT

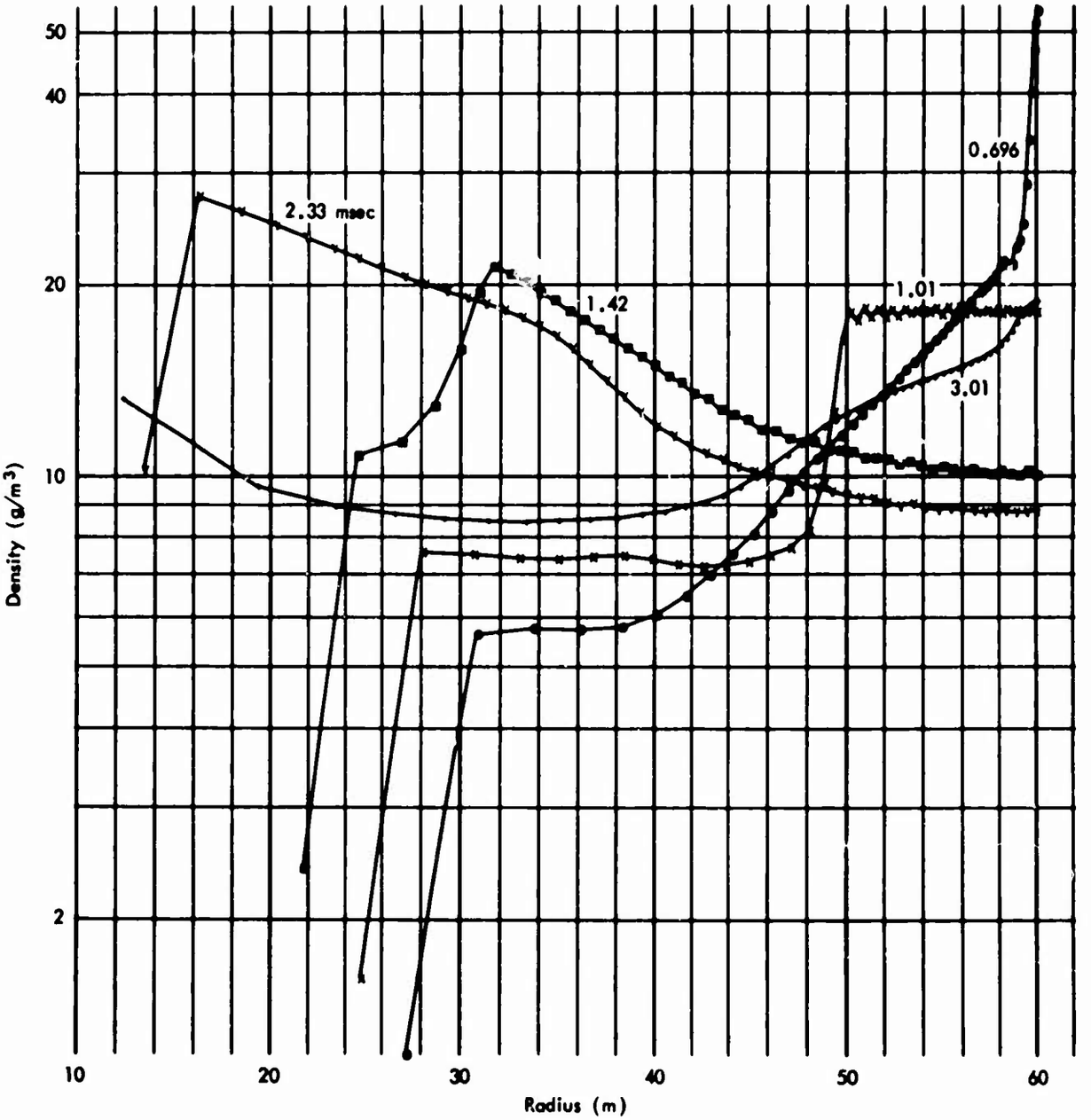

Fig. 30—Density profiles after first reflection, 60 m, 10 KT

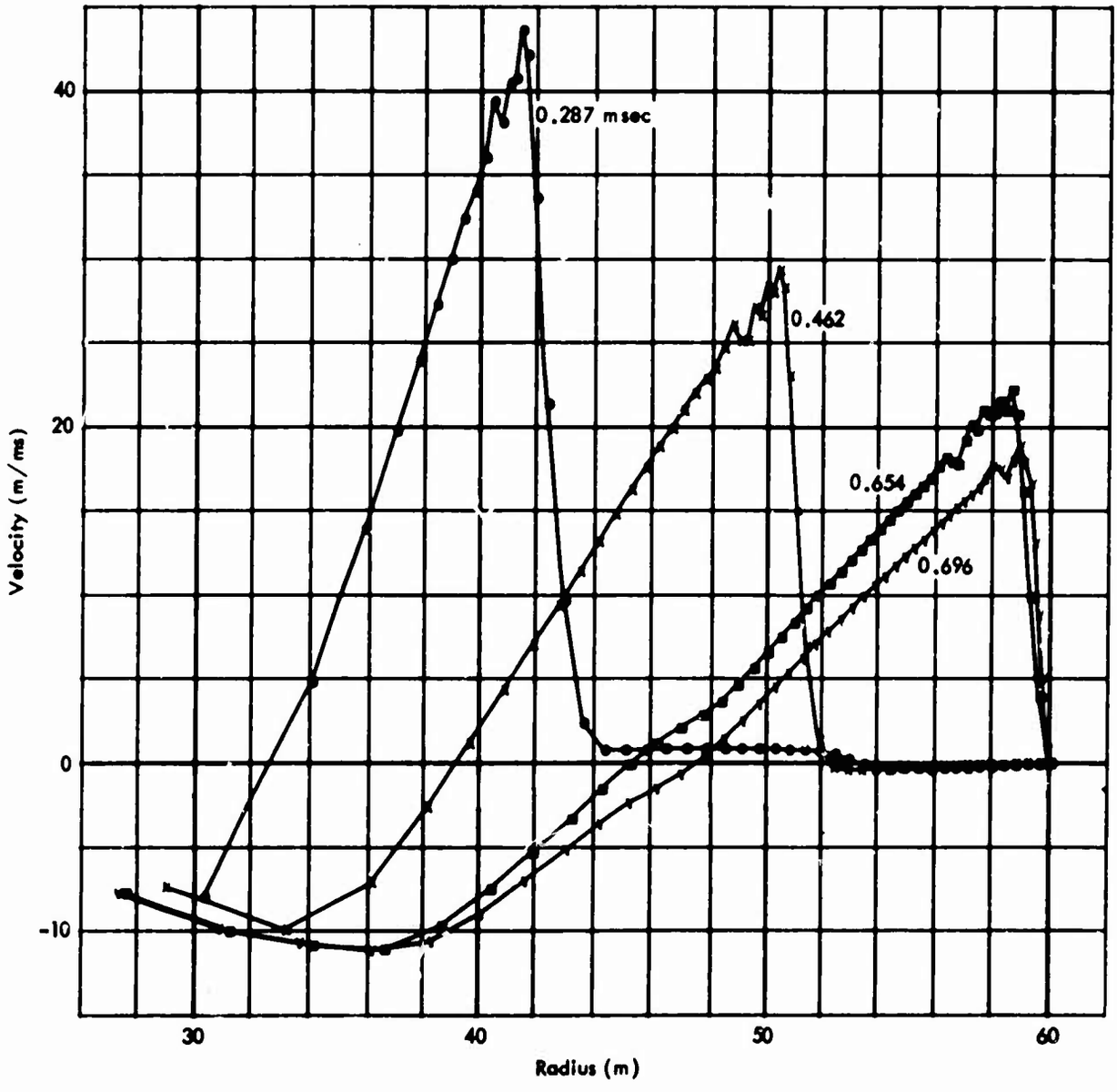

Fig. 31—Early velocity profiles, 60 m, 10 KT

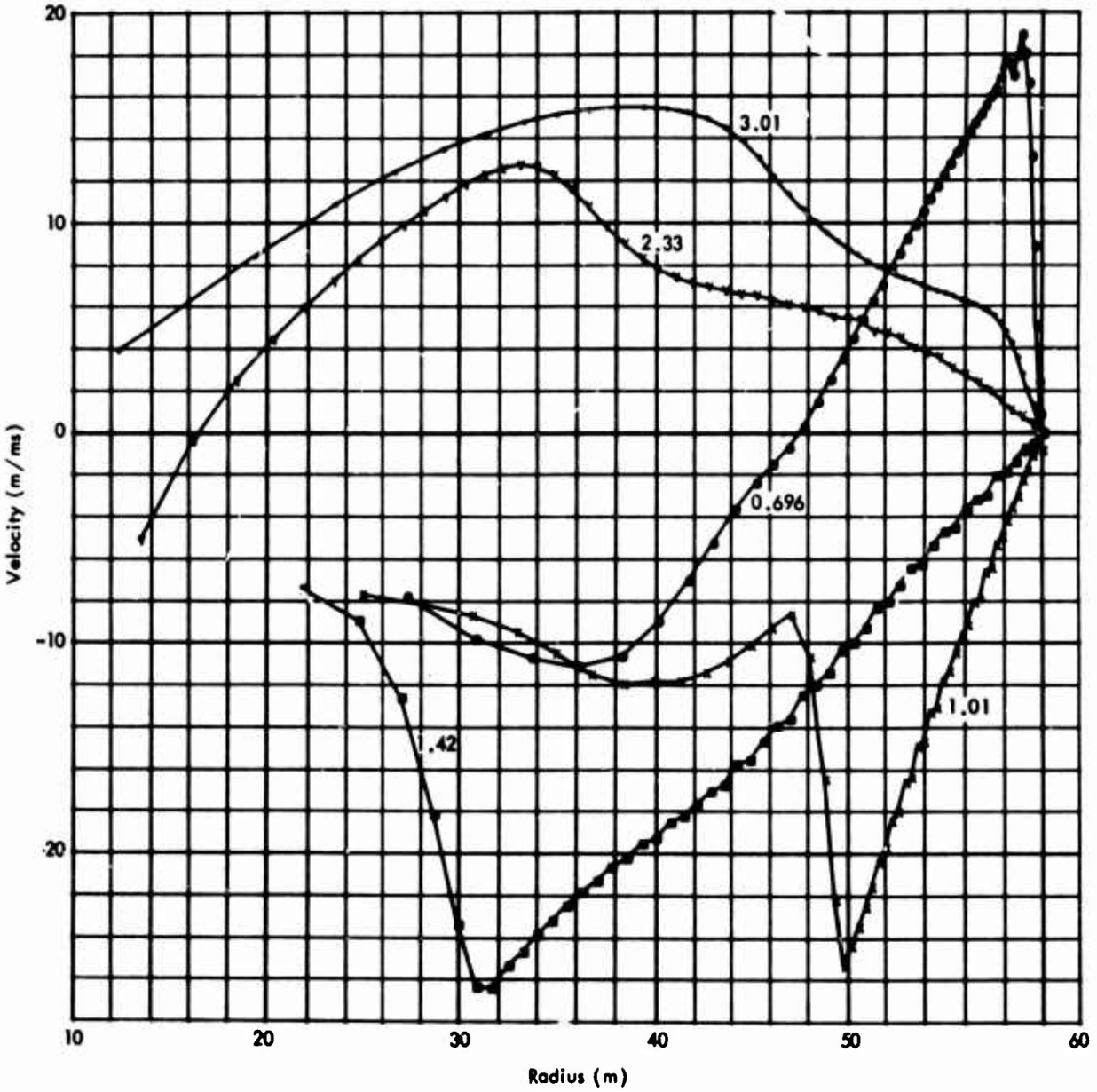

Fig. 32—Velocity profiles after first reflection, 60 m, 10 KT

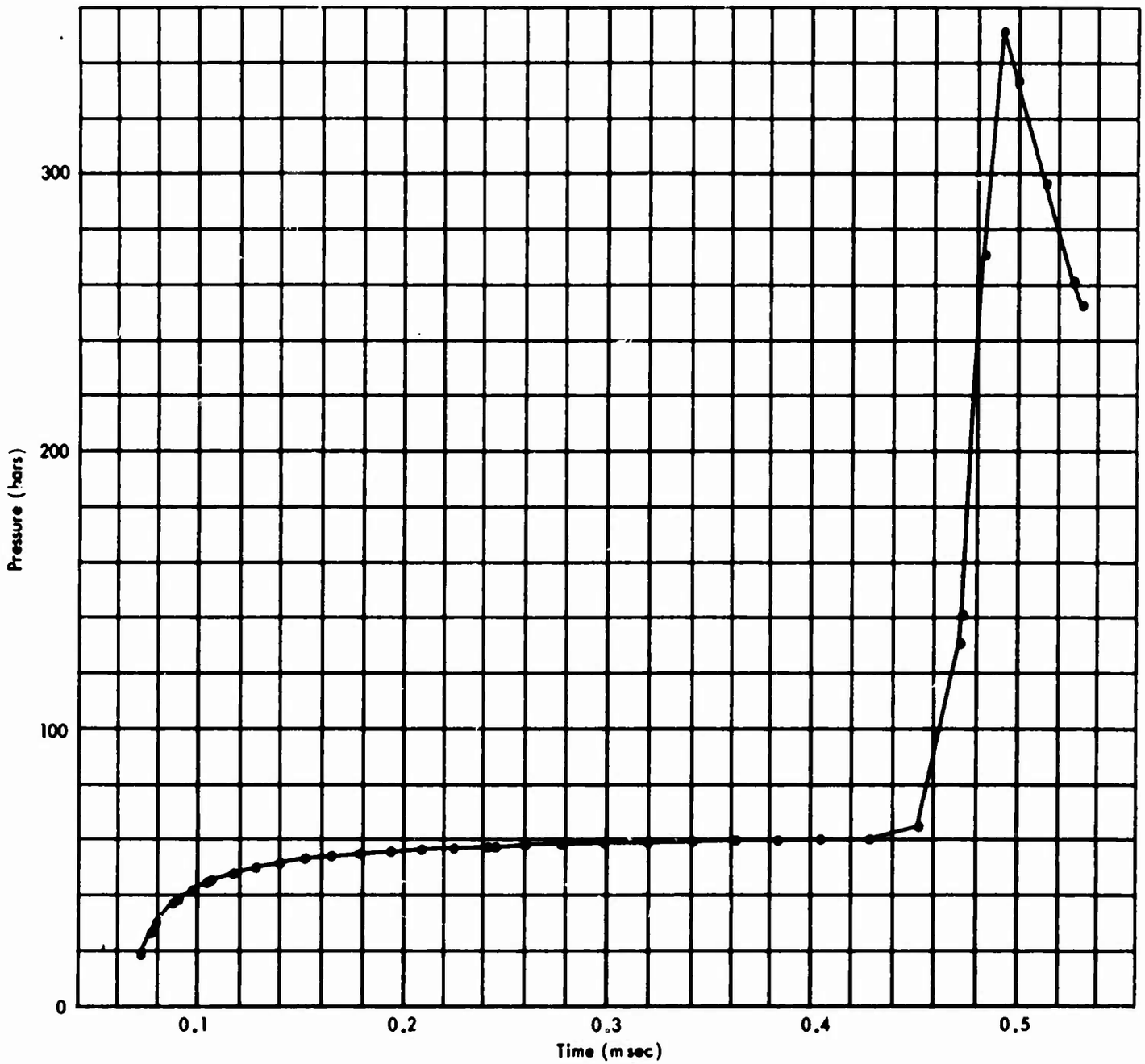

Fig. 33—Wall pressure versus time, 40 m cavity, 1.7 KT, 1/2 mass source

Fig. 34—Gas density at wall versus time, 40 m, 1.7 KT, 1/2 mass source

the wall (Fig. 35) has already leveled off at near the isothermal value when the shock arrives, so that little change accompanies the reflection.

Pressure, temperature, and density profiles for this case are shown in Figs. 36, 37, and 38, respectively. The rapid approach to a uniform temperature is obvious. Figure 39 extends the wall pressure history to 16.5 msec, showing the oscillatory behavior of the shocks in the now isothermal cavity gas.

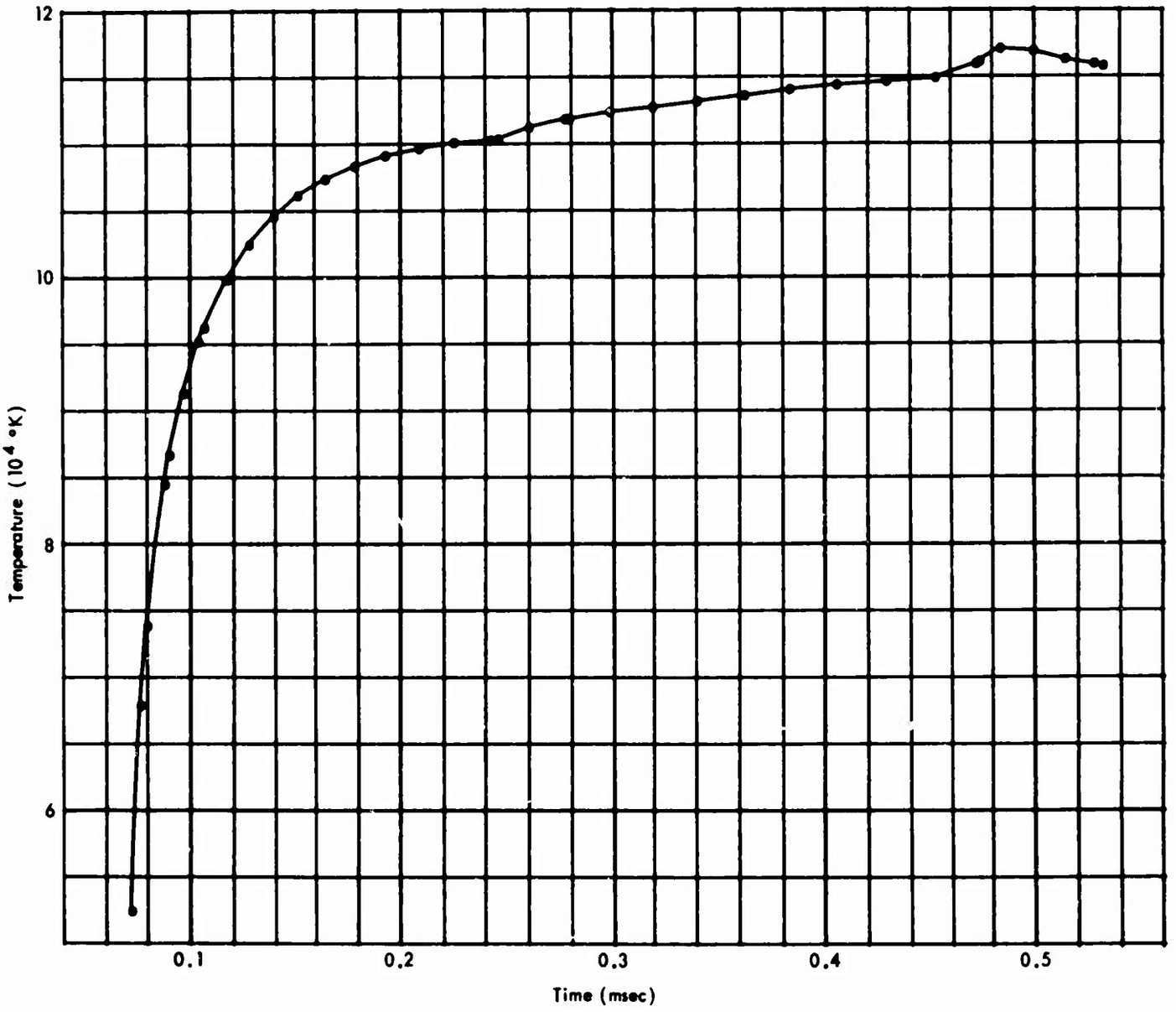

Fig. 35—Gas temperature at wall, 40 m, 1.7 KT, 1/2 mass source

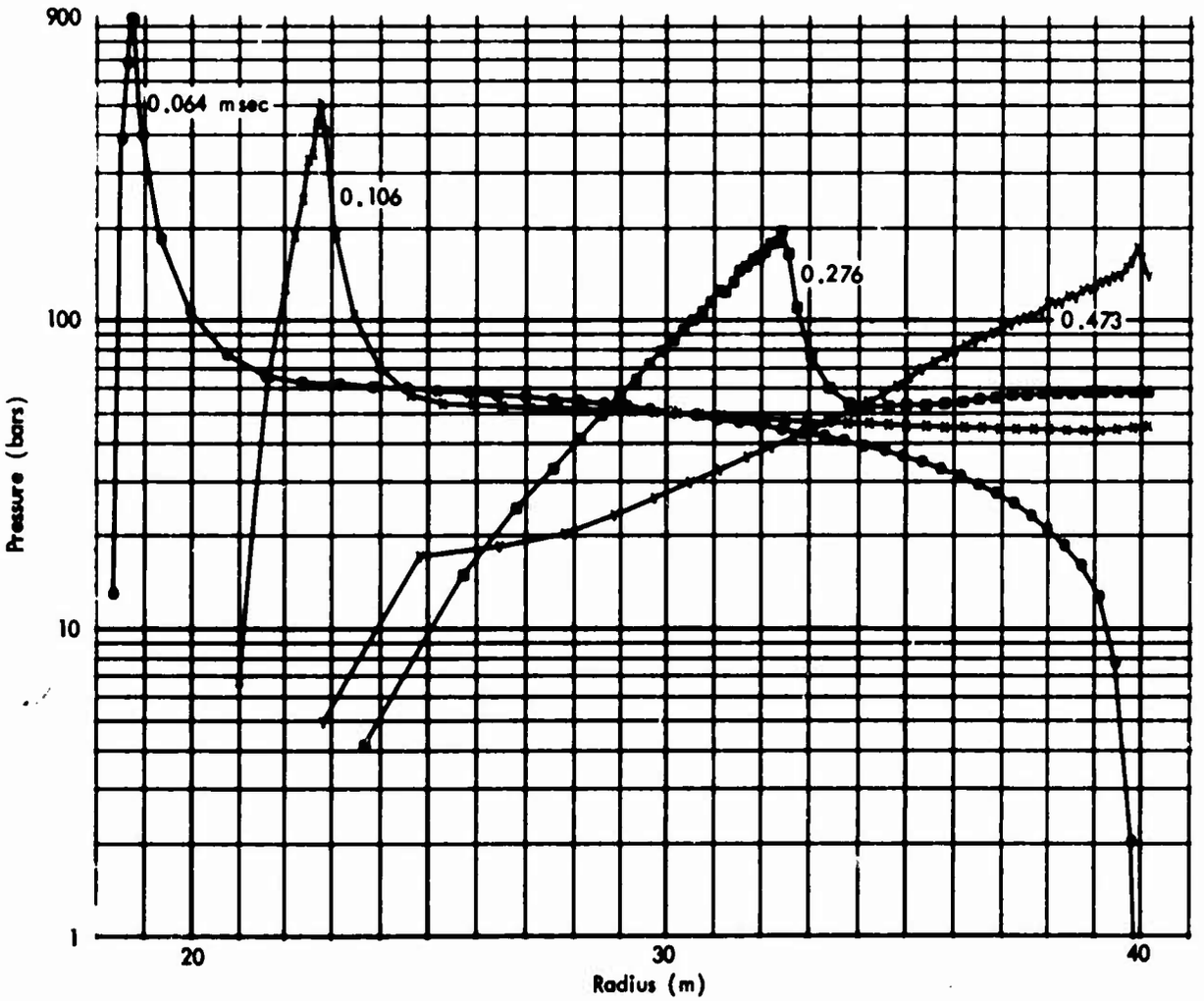

Fig. 36—Pressure profiles, 40 m cavity, 1.7 KT, half-mass source

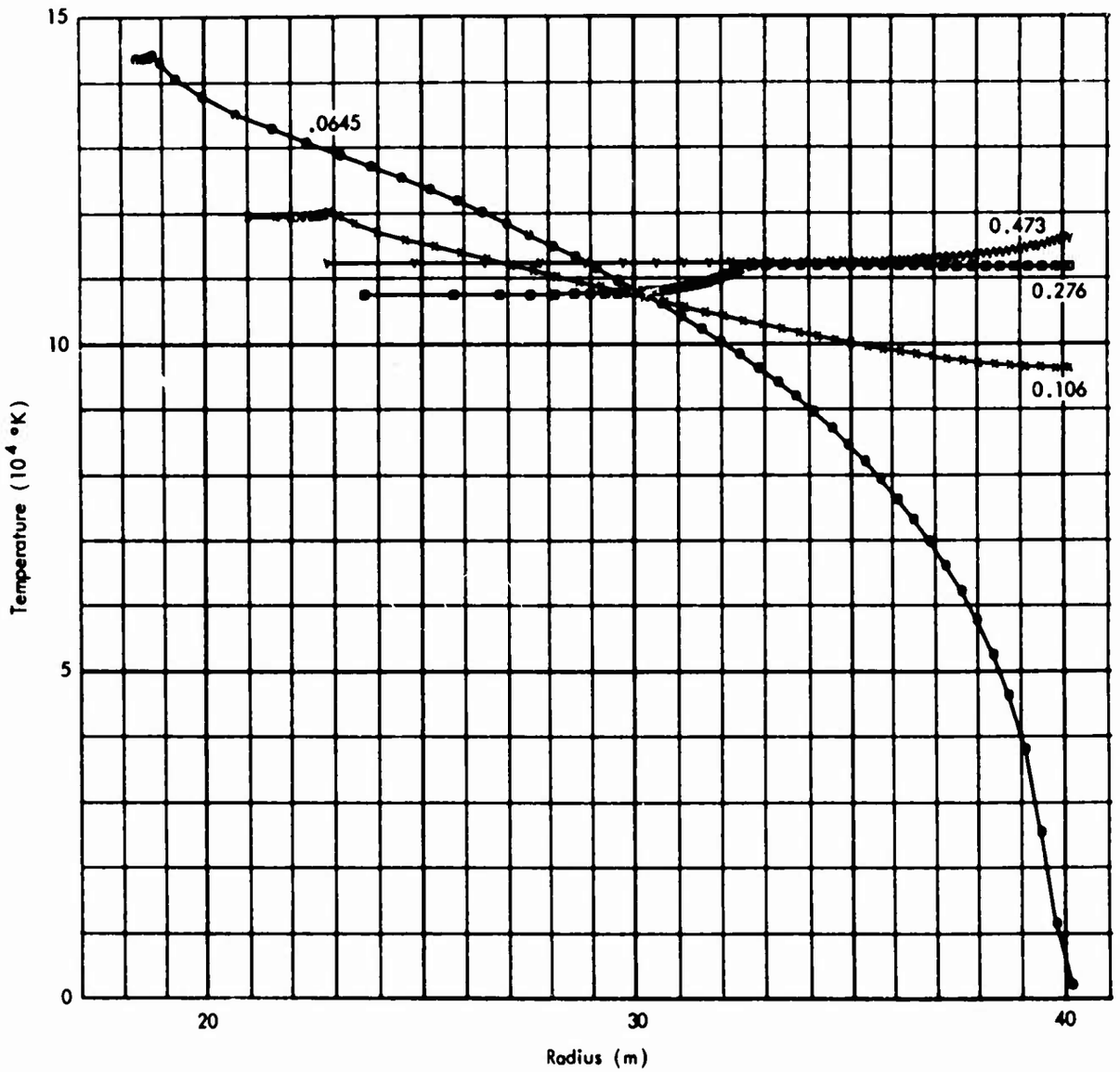

Fig. 37—Temperature profiles, 40 m cavity, 1.7 KT, half-mass source

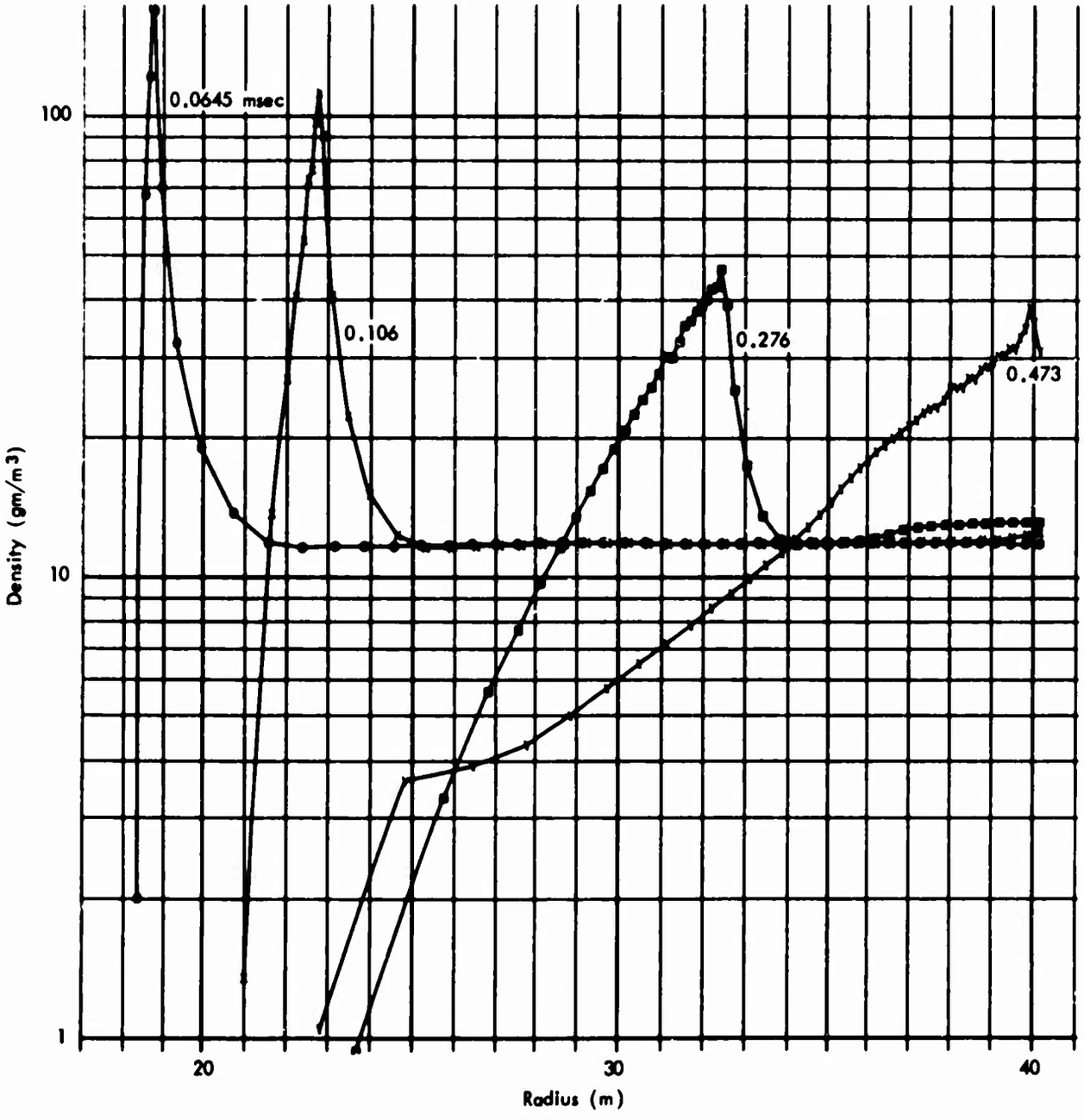

Fig. 38—Density profiles, 40 m cavity, 1.7 KT, half-mass source

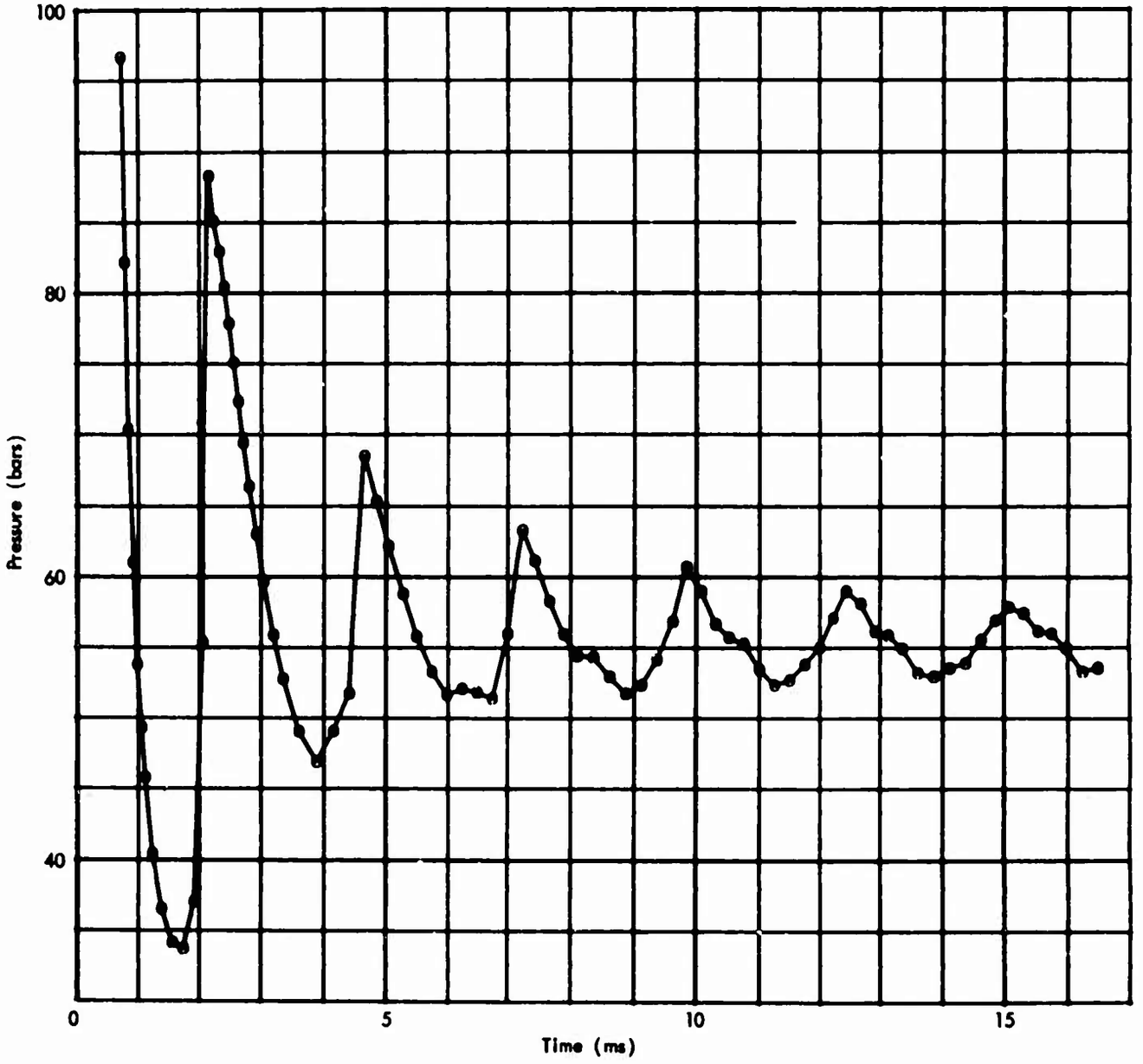

Fig. 39—Late wall pressure history, 40 m cavity, 1.7 KT, half-mass source

V. SUMMARY

The table below summarizes certain features of the various calculation results. The peak pressure, temperature, and density ratio of the cavity gas is listed for each case. The incident shock pressure and temperature are listed where appropriate. The frequency of cavity oscillation (reciprocal of the period between shocks on the wall) is an approximate average, and is not well-defined for all problems. The average pressure and temperature listed in each case is a rough estimate from late time listings, and is not always the same as the true average defined by the total energy, total gas mass and equation of state. The pressure and temperature at the wall ahead of the shock sometimes rises due to the radiation diffusion wave. It does not rise in the larger cavity and higher gas density cases, since the case shock overtakes the radiation-driven front in those examples. In such cases where the radiation precursor exists, the reflection is perturbed, and the incident pressure and temperature plays a role. It is of some interest to compare the ratios of reflected and incident pressures at the wall, and to compare the peak reflected pressures and temperatures with those at the radiation front and with the incident shock both when a wall is present to confine the radiation and without a wall.

It is clear that even for these low yield examples, radiation plays an important role, and the radiative properties of the cavity gas (water vapor) as well as the nuclear source vapors (only aluminum, in these examples) need more careful definition. General features, however, should be as described here.

Table 1

NUCLEAR EXPLOSIONS IN CAVITIES -- CALCULATIONAL SUMMARY

Cavity Radius (m)	20*	20*	40*	40*	40*	40	40	60	60	80
Cavity Contents	Air	Air	Air	Air	Air	Water	Water	Water	Water	Water
Cavity Gas Density(g/m^3)	1293	129	1293	129	12.9	11.8	11.8	11.8	11.8	11.8
Yield (KT)	1.7	1.7	1.7	1.7	1.7	1.7	1.7	1.7	10	1.7
Peak Wall Pressure(bars)	8200	3300	750	1040	189	676	350	157	383	137
Peak Wall Temperature (10^4 °K)	2.9	12.5	0.65	3.4	13.0	12.2	11.7†	5.5	16.94†	1.86
Peak Compression at Wall $((\rho-\rho_a)/\rho_a)$	27	11.5	27.2	30	3.32	11.76	5.75	7.46	53.4	35.8
Average Pressure	420	400	55	52.5	44	56.7	55	16	~ 90	~ 8
Average Temperature	9.4	12	3.5	4.4	12.8	11.68	11.58†	4.8	16.94†	~ 2.2
Radiation Wave Pressure at Wall (Bars)	---	---	---	---	~ 40	~ 53	~ 56	13.5	89	---
Radiation Wave Temperature at Wall (10^4 °K)	---	---	---	---	~ 13†	~ 10.5	~ 11†	2.86	16.94†	---
Incident Shock at Wall (Bars)	700	1000	90	84	100	204	146	~ 76	~ 185	124
Incident Shock Temperature (10^4 °K)	1.16	10	.37	12.8	13†	11.6	11.4	5.25	16.94†	0.94
Frequency of Ringing (cps)	420	810	67	160	380	275	385	220	350	---

†Cavity isothermalized early.

*See Reference 1.

REFERENCES

1. Brode, H. L., Nuclear Explosions in Cavities, The RAND Corporation, RM-3727, November 1965, Unclassified.

2. Latter, A.L., R. LeLevier, E. Martinelli, W. McMillan, J. Geophys. Res., Vol. 66, March 1961, pp. 943-946.

3. Herbst, R.F., G.C. Werth, D.L. Springer, J. Geophys. Res., Vol. 66, March 1961, pp. 959-978.

4. Latter, A., E. Martinelli, J. Mathews, W. McMillan, J. Geophys. Res., Vol. 66, Sept. 1961, pp. 2929-2936.

5. Haskell, N.A., J. Geophys. Res., Vol. 66, Sept. 1961, pp. 2937-2944.

6. Whitener, J., A. Latter, E. Martinelli, The RAND Corporation, Private Communication.

7. Asano, W., H. L. Brode, M. Plemmons, L. Scantlin, A. Stevenson, A Program for Calculating Radiation Flow and Hydrodynamic Motion, The RAND Corporation, RM-5187-PR, April 1967, Unclassified.

8. Gilmore, F.R., Basic Energy-Level and Equilibrium Data for Atmospheric Atoms and Molecules, The RAND Corporation, RM-5201-ARPA, March 1967, Unclassified.

9. Papetti, R.A. and M. Fujisaki, The Rice and Walsh Equation of State for Water: Discussion, Limitations, and Extensions, The RAND Corporation, RM-5050-PR, December 1967, Unclassified.

10. Krieger, F.J., A Parametric Study of Certain Low-Molecular-Weight Compounds as Nuclear Rocket Propellants. III, Water, The RAND Corporation, RM-2402, July 31, 1959, Unclassified.

DOCUMENT CONTROL DATA

1 ORIGINATING ACTIVITY THE RAND CORPORATION	2a. REPORT SECURITY CLASSIFICATION UNCLASSIFIED 2b. GROUP
3. REPORT TITLE MORE NUCLEAR EXPLOSIONS IN CAVITIES	
4. AUTHOR(S) (Last name, first name, initial) Brode, H. L.	

5. REPORT DATE June 1968	6a. TOTAL No. OF PAGES 62	6b. No. OF REFS. 10
7. CONTRACT OR GRANT No. F44620-67-C-0045	8. ORIGINATOR'S REPORT No. RM-5685-PR	
9a. AVAILABILITY/LIMITATION NOTICES DDC-1	9b. SPONSORING AGENCY United States Air Force Project Rand	

10. ABSTRACT

An extension of earlier calculations (in RM-3727) describing cavity gas dynamics and wall pressures and temperatures for low-yield nuclear explosions to include 10-KT explosions, 40-, 60-, and 80-meter-radius cavities, and a contained atmosphere of water vapor at about 11 torr. These calculations do not include the effects of absorbers, but rather extend the previous results to larger cavity sizes, to lower ambient (pre-shot) cavity pressures, and to higher yields. Wall pressures, temperatures, and densities are reported for five new specific cases, with average cavity pressures ranging from approximately 8 to approximately 90 bars, and peak pressures ranging from 137 to 676 bars. Some typical pressure, temperature, and density profiles in the cavity interiors at various times are reported, in addition to the wall pressures, temperatures, and densities as functions of time for each case.

11. KEY WORDS

Physics
Nuclear control
Nuclear effects
Weapons effects
Testing